UNITED NATIONS UNIVERSITY
GEOTHERMAL TRAINING PROGRAMME
Orkustofnun, Grensásvegur 9,
IS-108 Reykjavík, Iceland

Reports 2007
Number 22

TRANSIENT ELECTROMAGNETIC AND MAGNETOTELLURIC GEOPHYSICAL METHODS IN THE HENGILL AREA, SW-ICELAND

Andemariam Teklesenbet
Ministry of Energy and Mines
Department of Mines, Geological Survey
P.O. Box 272, Asmara
ERITREA
andatus2@yahoo.com

ABSTRACT

Geophysical methods, particularly electrical resistivity methods, have been the most powerful tools in geothermal exploration for decades. Of these, TEM and MT methods are important electrical methods in outlining geothermal resources. TEM soundings have proven to be more downward focussed than the traditional DC-soundings and have a better resolution at depth. The resistivity structures of high-temperature geothermal systems in volcanic areas are generally characterized by a high-resistivity core below a low-resistivity cap.

In this project, existing TEM and MT data from the Hellisheidi geothermal field of the Hengill volcanic area were interpreted. An interpretation program called TEMTD was used to perform 1D inversion on the TEM and MT data and the results obtained used to make iso-resistivity maps and cross-sections to describe the resistivity distribution. The results from TEM show that there exists a high-resistivity core below a low-resistivity cap from about 500 m b.s.l. down to about 900 m b.s.l., and at as shallow a depth as ~ 100 m b.s.l. along the fissure swarm. The low-resistivity cap extends up to sea level and in the northern part of the study area, up to 100 m a.s.l. and even to the surface at some points. Moreover, results from MT data show that there is a low-resistivity structure at depth, at about 5000 m b.s.l. down to about 10,000 m b.s.l. that is interpreted as a heat source. The results from these resistivity surveys indicate that this area is potentially a good high-temperature area.

1. INTRODUCTION

Geophysics, particularly electrical resistivity methods, has been among the most powerful tools in geothermal exploration for decades. Using these methods, the physical properties of the earth's crust are examined. The main role and activity of geothermal exploration through the use of geophysics is to detect and delineate geothermal resources, and to locate exploitable reservoirs, and furthermore to site drill holes, through which hot fluids at depth can be extracted. Most of the geophysical methods have been applied in geothermal prospecting but the various electrical and thermal methods have been most important. Rocks containing geothermal fluids are usually characterized by anomalous low resistivity. The methods which can measure electrical resistivity at depth have been the most useful of all geophysical methods and are used to locate geothermal reservoirs. Geoelectrical resistivity

methods, in particular Transient Electro-Magnetic (TEM) and MagnetoTelluric (MT) methods, are here most important and key techniques in geothermal exploration.

In this project, existing TEM (106 soundings) and MT (47 soundings) from Hellisheidi geothermal field in the Hengill volcanic area were interpreted. 1D modelling using TEMTD Occam inversion was applied to interpret the data. The results are presented as iso-resistivity maps at different elevations as well as cross-sections from both TEM and MT soundings.

2. GEOPHYSICAL METHODS IN GEOTHERMAL EXPLORATION

2.1 Introduction

Studies and knowledge on major structures and lineaments helps to determine what geothermal conditions prevail in the underground. But that alone doesn´t tell you much about the dimensions of the source and its exact orientation. A realistic interpretation of structures and geological contacts requires some knowledge of geological formations and tectonic history. Some of this knowledge can be gained through geological mapping in areas where the units crop out on the surface; however, not all units appear on the surface. To reveal these hidden units and structures, geophysical methods are important. The main purpose of geophysical exploration in geothermal areas is to:

- find geothermal prospects;
- outline drilling fields;
- locate aquifers and site wells;
- estimate properties of the system.

For a geothermal reservoir to be classified as a good potential, it should have high porosity and permeability accompanied by high temperature.

2.2 Important geophysical methods for geothermal exploration

The most important physical properties of a geothermal system that geophysical methods can estimate are temperature, permeability and chemical composition of the fluid and formation. Depending on the methods, various parameters can be measured by geophysical exploration. Generally, geophysical methods are divided into two groups: direct methods (thermal and electrical methods) and indirect/structural methods (magnetic, gravity and seismic methods) (Hersir and Björnsson, 1991; Árnason and Flóvenz, 1992; Eysteinsson et al., 1993; Manzella, 2006):

Thermal methods: These are the most direct methods through studying the subsurface temperatures in a geothermal system. Heat exchange takes place through conduction and convection, and the temperature is measured in shallow drill holes or in soil. Estimation of the temperature at depth is made from the temperature gradients.

*Electrical methods***.** The main types are:

DC methods: In this technique, an electrical current is injected into the earth through electrodes and the resulting potential differences are measured at the surface. Several variations of the direct current resistivity method have been used for decades, but the most widely used in geothermal exploration is the Schlumberger array. Distinction is made between two different procedures: sounding and profiling, aimed at measuring resistivity changes with depth and lateral variations, respectively.

Electromagnetic methods: Both natural source electromagnetic MT and controlled source electromagnetic TEM are widely used. In the MT method, natural time variations in the earth´s magnetic field induce currents in the earth, and the electrical field induced is measured at the surface. This is a powerful method for determining resistivity distribution within the earth to depths of several tens or hundreds of kilometres. On the other hand, in the TEM method an artificial source is used to generate the electromagnetic field. The central loop TEM method was first tested for geothermal exploration in Iceland in the summer 1986 (Árnason, 1986), and has proven very useful in geothermal prospecting.

SP (self potential): This is another natural source electrical method and is a low-cost surveying technique. It has been applied in many geothermal areas; however, the anomalies are hard to interpret.

Magnetic methods: This is a structural method that has the ability of locating narrow linear features like dikes and faults which are covered by soil. It is useful in mapping near surface rock formations that are often of interest in geothermal areas.

Gravity survey: A structural method used during geothermal exploration to define lateral density variations related to deep magmatic bodies which may represent the heat source. This method is also used to define structures (like faults) and change in groundwater level and monitoring of mass balance in exploited geothermal systems.

Seismic methods: These methods are divided into two main subclasses. 1) Passive seismic methods which deal with the effect of natural earthquakes, and those induced by fracturing related to geothermal fluid extraction and injection. 2) The active seismic methods, which cover seismic prospecting, and have an artificial wave source.

Geophysical well loggings and borehole methods: These are valuable tools for direct exploration and detection of physical parameters which can then be extrapolated by surface geophysical methods. For direct exploration, well logging identifies the permeability, in particular fractures, and the nature of the fluid present.

3. ELECTRICAL RESISTIVITY OF ROCK FORMATIONS

Electrical resistivity is the extent to which the flow of electricity is hindered when passing through a particular material.

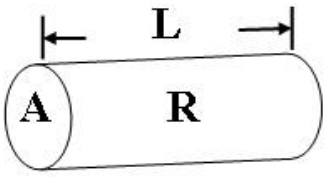

FIGURE 1: Parameters used to define resistivity

For a conducting material of resistance R, length L and cross-sectional area A (Figure1), the electrical resistivity ρ (rho) of that material is given by the equation:

$$\rho = \frac{RA}{L} \tag{1}$$

where ρ = Resistivity (Ωm);
R = Electrical resistance (Ω);
A = Cross-sectional area (m^2);
L = Length (m).

For most rocks the electrical resistivity is greatly influenced by the following rock properties:

- Porosity (intergranular and fracture) and permeability;
- Amount of water (pore fluid saturation);
- Pore fluid resistivity (salinity of the water);
- Temperature;
- Water-rock interaction and alteration; and
- Steam content in the water.

Electrical resistivity of rocks is most sensitive to the nature and amount of pore saturant, temperature and alteration.

3.1 Porosity and permeability of rock formations

Porosity and permeability are related properties of any rock or loose sediment. Both are related to the number, size, and connections of rock openings. Mathematically, *porosity* is the open space in a rock divided by the total rock volume (solid and space). It can be inter-granular in nature consisting of the space left over after the rock grains were compacted. In other rocks, porosity occurs primarily in the form of joints. A third form of porosity, common in limestone and in some volcanic rocks, is vugular porosity consisting of larger, irregular cavities formed either by solution, as in limestone, or by larger gas bubbles as in volcanic rocks (Keller and Frischknecht, 1966).

Resistivity of water-bearing rocks depends on the amount of water present. It has been observed that resistivity varies approximately as inverse powers of the porosity when the rock is fully saturated with water (Keller and Frischknecht, 1966). This observation has led to the widespread use of an empirical function relating resistivity and porosity which is know as Archie´s law, given by the formula (Archie, 1942):

$$\rho = a\rho_w \varphi^{-m} \tag{2}$$

where ρ = Bulk resistivity (Ωm);
ρ_w = Resistivity of the pore fluid (Ωm);
φ = Porosity expressed as a fraction per unit volume of rock;
a = Empirical parameter that varies from less than 1 for inter-granular porosity to slightly more than 1 for rocks with joint porosity;
m = A parameter somewhat larger than 2 for cemented and well sorted granular rocks and somewhat less than 2 for poorly sorted and poorly cemented granular rocks.

Equation 2 is often expressed as:

$$\rho = \rho_w F \tag{3}$$

where F is the so-called formation factor, $F = a\,\varphi^{-m}$

Permeability is a measure of the ease of fluid flow through a porous solid. A rock may be highly porous, but if the pores are not connected, it will have no permeability. Likewise, a rock may have a few continuous cracks which allow easy fluid flow, but when porosity is calculated, the rock doesn't seem very porous.

3.2 Resistivity as a function of salinity

As mentioned in the previous section, the bulk resistivity of a rock is often controlled mainly by the resistivity of the pore fluid, which in itself depends critically on the salinity of the fluid. How fluid conductivity ($\sigma = 1/\rho$) varies with salinity is shown in Figure 2. An increase in the amount of

dissolved ions in the pore fluid increases the conductivity. Conductivity of solutions is a function of salinity and the mobility of the ions present in the solution. This is expressed in the following equation (Hersir and Björnsson, 1991):

$$\sigma = \frac{1}{\rho} = F(c_1 q_1 m_1 + c_2 q_2 m_2 + \cdots) \quad (4)$$

where σ = Conductivity (S/m);
F = Faraday´s number (9.65×10^4 C);
c_i = Concentration of ions;
q_i = Valence of an ion;
m_i = Mobility of an ion.

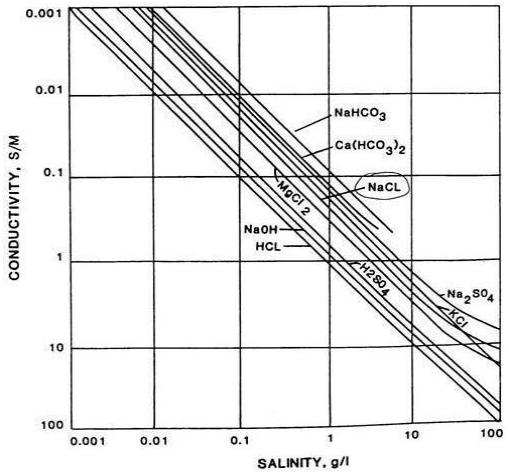

FIGURE 2: Pore fluid conductivity vs. salinity (concentration for a variety of electrolytes) (mod. from Keller and Frischknecht, 1966)

3.3 Resistivity as a function of temperature

Extreme range in temperature affects the resistivity of water-bearing rocks. High temperatures drive water from the rock as steam; at low temperatures, the water in the pores of the rock freezes. At moderate temperatures, the resistivity of the pore fluid decreases with increasing temperature. This is because the mobility of the ions in solution increases with a decrease in the viscosity of the water caused by the increase in temperature. The dependence of resistivity on temperature for aqueous solutions from 0°C to about 200°C is approximated by Dakhnov (1962) with:

$$\rho_w = \frac{\rho_{w_0}}{1+\alpha(T-T_0)} \quad (5)$$

where ρ_{wo} = Resistivity of the fluid at temperature T_o (Ωm);
α = Temperature coefficient of resistivity (°C^{-1}),
≈ 0.023°C^{-1} for T_o = 23°C, and
0.025°C^{-1} for T_o = 0°C

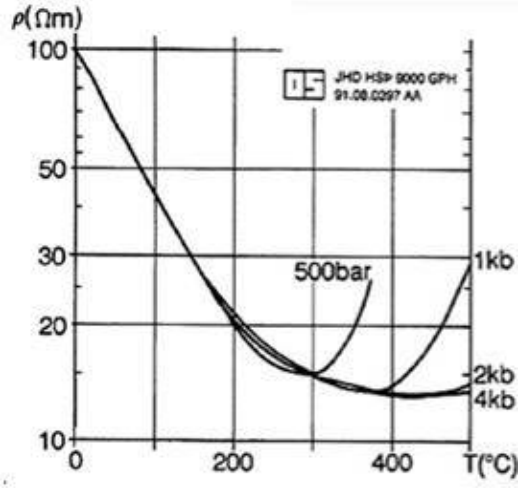

FIGURE 3: Resistivity of an electrolyte as a function of temperature

At high temperatures, a decrease in the dielectric permittivity of the water results in a decrease in the number of dissociated ions in solution. Above 300°C, this starts to increase fluid resistivity as in Figure 3.

3.4 Resistivity and fluid rock interaction

Experiments show that Archie´s law is only valid for conductive solutions, $\rho_w \leq 2$ Ωm (Flóvenz et al., 1985). The bulk resistivity is decreased by surface conduction along the interface between rock and water. This can be expressed in a formula (Rink and Schopper, 1976) as:

$$\sigma = \left({}^{1}/_{F}\right) \cdot \sigma_w + \sigma_s \quad (6)$$

where σ = Bulk conductivity (S/m);
F = Formation factor;

σ_w = Conductivity of water (S/m);
σ_s, = Interface conductivity (S/m).

The interface conductivity, σ_s, is caused by fluid-matrix interaction and for resistive fluids it may dominate. Experiments show that interface conductivity depends on the magnitude of the internal surface (porosity), its nature (surface conditions) as well as temperature and chemical composition of water and rock. The two main reasons for interface conductivity are the presence of alteration minerals and surface double layer conduction. Surface resistivity surveys of high-temperature geothermal systems of volcanic areas reveal the existence of a low-resistivity cap over a high-resistivity core. Comparisons of resistivity structures with data from wells were carried out in high-temperature geothermal areas in Iceland (Árnason et al., 2000) and in the Asal Rift, Djibouti East Africa (Árnason et al., 1988). The results were in good agreement with alteration mineralogy.

In the Icelandic high-temperature geothermal areas, at temperatures below 200°C, smectites and zeolites are the dominant alteration minerals but chlorite and epidote predominate above 250°C. Between 200°C and 250°C, there is a transition called the mixed layer zone (Árnason et al., 1987; Árnason and Flóvenz, 1992).

The resistivity is relatively high in cold unaltered rocks outside the reservoir. The low-temperature alteration mineralogy, the smectite-zeolite zone, forms a low-resistivity cap at the outer margin of the reservoir and the upper boundary of this low-resistivity cap corresponds to temperatures in the range of 50-100°C, depending on the intensity of the alteration. The transition from the low-resistivity cap to the resistive core corresponds to temperature in the range of 230-250°C. The resistivity increases again towards the interior of the reservoir at the top of, or within, the mixed layer clay zone. If the temperature is in equilibrium with the dominant alteration mineralogy, then the resistivity structure can directly correlate with temperature.

Usually resistivity decreases with increasing temperature but in high-temperature volcanic areas the situation is the reverse in the chlorite and chlorite-epidote alteration zone; i.e., resistivity increases with increasing temperature. The reason for this transition is that smectite and zeolites have mobile ions. In the higher temperature alteration minerals, these ions are fixed in the crystal lattice.

4. THE CENTRAL-LOOP TRANSIENT ELECTROMAGNETIC METHOD

4.1 Basic theory

In the central-loop TEM sounding method, a current is induced in the ground by a time-varying magnetic field of a controlled magnitude generated by a source loop. A loop of wire is placed on the ground and a constant magnetic field of known strength is built up by transmitting a constant current into the loop (Figures 4). The current is then abruptly turned off. The decaying magnetic field induces electromotive forces in the ground. The induced current is initially concentrated below the transmitter loop, but then the current diffuses down and away from the transmitter (Figure 5). The current distribution in the ground generates a secondary magnetic field that decays with time. The decay rate of the secondary magnetic field as a function of time is monitored by measuring the voltage induced in a receiver coil at the centre of the transmitting loop in time gates (Figure 4biii). The current distribution and the decay rate of the secondary magnetic field depend on the resistivity structure of the earth. The decay rate, recorded as a function of time after the current in the transmitter loop is turned off, can therefore be interpreted in terms of the subsurface resistivity structure (Árnason, 1989).

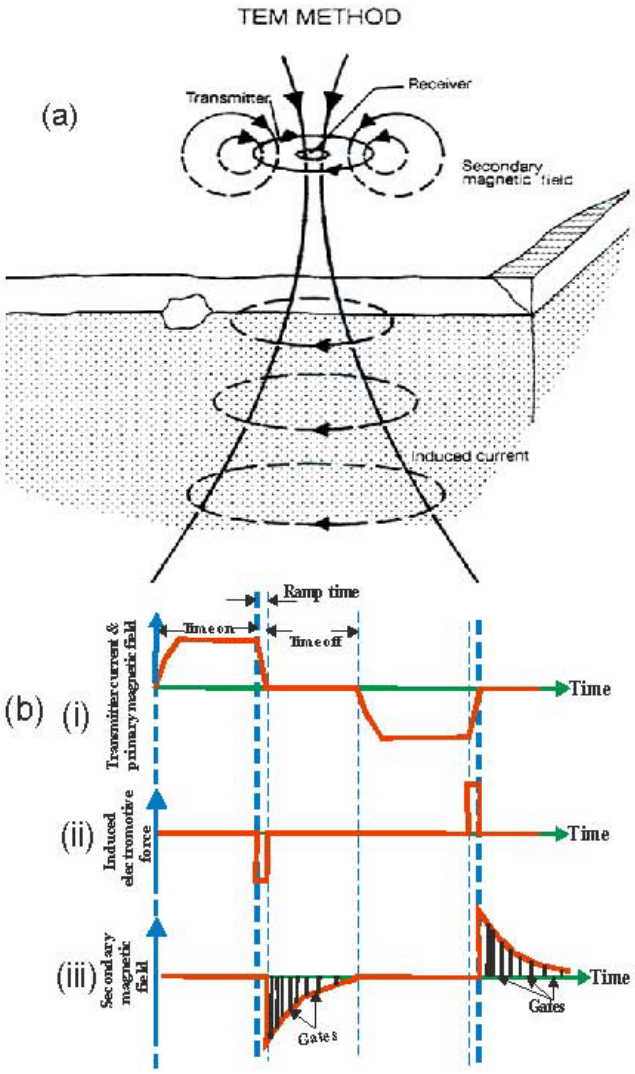

FIGURE 4: The central loop TEM configuration (mod. from Hersir and Björnsson, 1991)

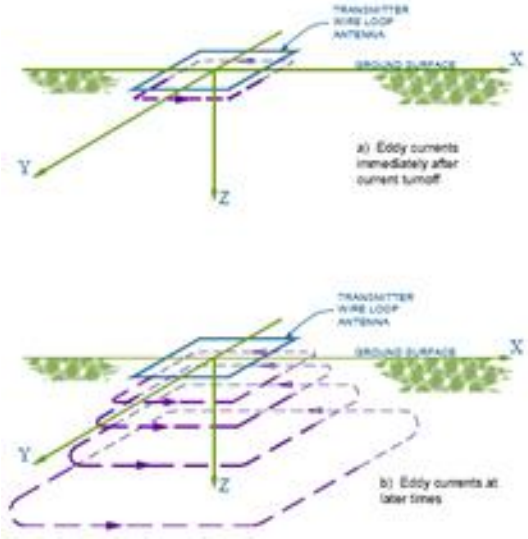

FIGURE 5: TEM eddy current flow; a) Early time; b) Late time (McNeill, 1980)

4.2 Layered earth

The induced voltage in a receiver coil at the centre of a circular source loop with a radius r with the harmonic current, $I = I_0 e^{i\omega t}$ on the surface of an N-layered half-space is given as (Árnason, 1989):

$$V(\omega, r) = A_r n_r A_s n_s \, I_0 e^{i\omega t} \frac{-i\omega\mu}{\pi r} \int_0^\infty \frac{\lambda^2}{m_0} \frac{S_0}{S_0 - T_0} J_1(\lambda r) d\lambda \qquad (7)$$

where A_r = Cross-sectional area of the receiver coil (m^2);
n_r = Number of windings in the receiver coil;
μ_0 = Magnetic permeability in vacuum (H/m);
A_s = Cross-sectional area of the transmitter loop (m^2)
n_s = Number of windings in the transmitter loop;
r = Radius of transmitter loop (m).

S_0 and T_0 ,which depend on layer resistivity and thickness, are given by the recursion relationships:

$$S_{i-1} = \cosh\,(m_i\, d_i) - T_i \sinh(m_i d_i) \qquad (8)$$

$$T_{i-1} = -\frac{m_i}{m_{i-1}}[S_i \sinh(m_i d_i)] - T_i \cosh(m_i d_i) \quad (9)$$

$$S_{N-1} = 1; \qquad T_{N-1} = \frac{m_N}{m_{N-1}}$$

where d_i = Thickness of the i^{th} layer (m); and
m_i = Impedance of the i^{th} layer.

The quantities S_0 and T_0 ,which determine the voltage in Equation 7, depend on angular frequency, ω and the conductivities, σ_i through $m = \sqrt{\lambda^2 - k_i^2}$ where $k_i^2 = \omega^2\mu_i\varepsilon_i - i\omega\mu_i\sigma_i$ (ε is the dielectric permittivity); i = 0, 1 …N. In the quasi-stationary approximation $\varepsilon \approx 0$, hence, $k^2 = i\omega\mu\sigma$.

Mutual impedance between the source and the receiver coil (by analogy with Ohm's law) is defined by the ratio between the measured voltage and the transmitted current. From Equation 7, the mutual impedance is:

$$Z(\omega, r) = \frac{V(\omega,r)}{I_0\, e^{i\omega t}} = A_r n_r A_s n_s \frac{-i\omega\mu}{\pi r} \int_0^\infty \frac{\lambda^2}{m_0} \frac{S_0}{S_0 - T_0} J_1(\lambda r) d\lambda \quad (10)$$

Equation 10 can be transformed to the time domain by Fourier expansion of the function describing the transmitted current (Árnason, 1989). If the transmitted current is described by the function *I(t),* a Fourier expansion of the current function will be:

$$I(t) = \frac{1}{(2\pi)^{1/2}} \int_{-\infty}^{\infty} \tilde{I}(\omega) e^{i\omega t}\, d\omega \quad (11)$$

where

$$\tilde{I}(\omega) = \frac{1}{(2\pi)^{1/2}} \int_{-\infty}^{\infty} I(t) e^{-i\omega t}\, dt$$

From Equation 11, the induced voltage in the receiver coil in terms of mutual impedance (as a function of frequency) and the Fourier transform of the transmitted current are expressed as:

$$V(t, r) = \frac{1}{(2\pi)^{1/2}} \int_{-\infty}^{\infty} Z(\omega, r)\, \tilde{I}(\omega) e^{i\omega t}\, d\omega \quad (12)$$

For a constant current I turned off at t = 0, $\tilde{I}(\omega) = -I_o/i\omega$. The measured voltage as a function of time after the steady current is abruptly turned off at t = 0 is then expressed by:

$$V(t) = \frac{-I_0}{2\pi} \int_{-\infty}^{\infty} \frac{Z(\omega)}{i\omega} e^{i\omega t}\, d\omega = \frac{I_0}{2\pi} \int_{-\infty}^{\infty} \Phi(\omega) e^{i\omega t}\, d\omega \quad (13)$$

where for convenience $\Phi(\omega)$ is defined as:

$$\Phi(\omega) = \frac{Z(\omega)}{-i\omega} \quad (14)$$

$\Phi(\omega)$ depends on ω through ω^2 and $i\omega$, hence:

$$\Phi^*(-\omega) = \Phi(\omega) \quad (15)$$

where * denotes the complex conjugation.

Hence:

$$\text{Re}\, \Phi(-\omega) = \text{Re}\, \Phi(\omega); \quad \text{Im}\, \Phi(-\omega) = \text{Im}\, \Phi(\omega) \quad (16)$$

This can be used to simplify Equation 13 because if it is written in terms of real and imaginary parts, it becomes:

$$V_{-}(t) = \frac{-2I_0}{\pi} \int_0^{\infty} \text{Re}\, \Phi(\omega)\cos(\omega t)\, d\omega, \quad \text{or} \quad V_{-}(t) = \frac{-2I_0}{\pi} \int_0^{\infty} \text{Im}\, \Phi(\omega) \sin(\omega t) d\omega \qquad (17)$$

In practice the current is not abruptly turned off, but turned off linearly (Figure 4bi) in a time interval of length *TOFF*. Transient voltage generated in the receiver coil due to a linearly ramped step function is given by (Árnason, 1989):

$$V(t) = \frac{I_0}{TOFF} \int_{-TOFF}^{0} V_{-}(t-\tau)\, d\tau = \frac{I_0}{TOFF} \int_{t}^{t+TOFF} V_{-}(-\tau) d\tau \qquad (18)$$

For a homogeneous half-space of conductivity σ, the induced voltage in the receiving coil, at late time after current turn-off, is given approximately by (Árnason 1989):

$$V(t,r) \approx \frac{C}{10\pi^{1/2}} \frac{(\mu_0 \sigma r^2)^{3/2}}{t^{5/2}} \quad \text{where} \quad C = A_r n_r A_s n_s \frac{\mu_0}{2\pi r^3} \qquad (19)$$

This can be solved to obtain the resistivity at the half-space. The formula is then for non-homogeneous earth used to define the so called late-time apparent resistivity (Árnason 1989):

$$\rho_a = \frac{\mu_0}{4\pi} \left[\frac{2\mu_0 A_r n_r A_s n_s}{5t^{5/2} V(t,r)} \right]^{2/3} \qquad (20)$$

where t = Time elapsed after the transmitter current is turned to zero (s); and
$V(t, r)$ = Measured voltage (V).

All other parameters are the same as described in Equation 7.

4.3 Homogenous earth

Voltage response of homogenous half spaces with different resistivities has the same general character and can be divided into three stages as in Figure 6. In the early stage, the induced voltage is constant in time. In the intermediate stage, the voltage starts to decrease with time and with steadily increasing slope on log-log scale until the late stage is reached. Then the voltage response decreases with time in such a way that the logarithm of the induced voltage decreases linearly as a function of the logarithm of time. The slop of the response curve in the late stage is easily seen to be -5/2 showing that the voltage is proportional to $t^{-5/2}$ (Equation 19). From Figure 6, we can also observe that the early stage voltage response increases with increasing resistivity of the half space. Also, the transitions from early to intermediate and from intermediate to late stages get shifted

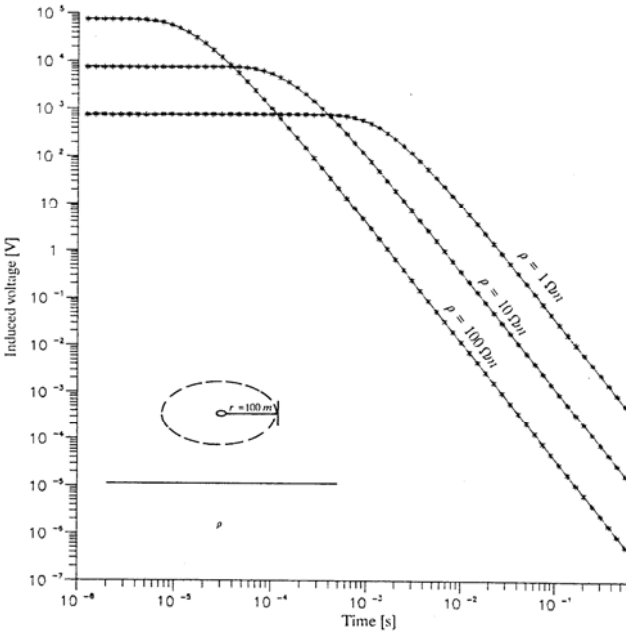

FIGURE 6: Voltage response for homogenous half space (mod. from Árnason, 1989)

towards earlier times but in such a way that the response curve has the same shape.

For a homogenous earth of resistivity ρ, the apparent resistivity (Equation 20) gives the true resistivity at late times. This can be seen from Figure 7 where the transient response for uniform half-space with resistivities, ρ = 1, 10 and 100 Ωm and for r = 100 m are shown as an apparent resistivity vs. time according to Equation 20 (Árnason, 1989). From Figure 7 it can also be seen that the apparent resistivity approaches the true resistivity of the half-space at later times as the resistivity gets lower.

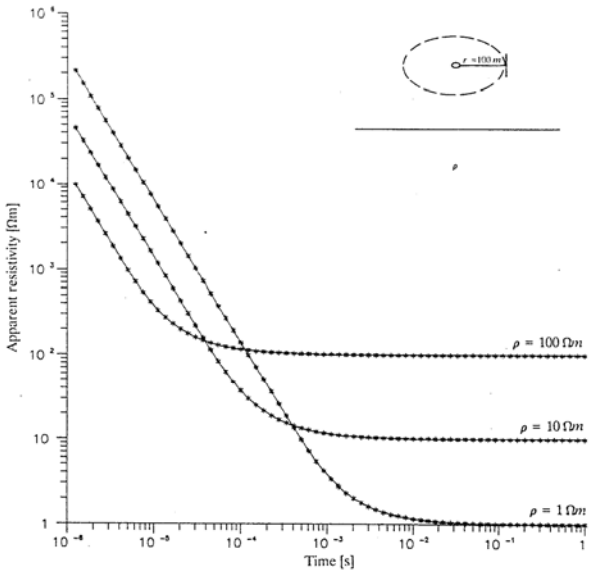

FIGURE 7: Late time apparent resistivity for homogenous half space (mod. from Árnason, 1989)

5. MAGNETOTELLURIC RESISTIVITY METHOD IN GEOTHERMAL EXPLORATION

5.1 Basic theory

The magnetotelluric method is a broad-frequency band (10^{-4}-10^{3} Hz) passive electromagnetic technique, which uses natural time-dependent variations in the earth´s magnetic field as the source, and an electric field induced in the earth as the response. The high frequency range (> 1 Hz) which originates from thunderstorm activities at the equator, is used to investigate resistivity variations of the upper crust. The low frequency range (< 1 Hz) called micro pulsations which originate by solar wind interacting with earth´s magnetic field and ionosphere, is used for deep crustal investigations. The data (time-series) are Fourier transformed to the frequency domain and processed to derive the impedance tensors which, in turn, are used to derive apparent resistivities and phases. Lastly the resistivity distribution within the earth to depths of many kilometres is determined from them.

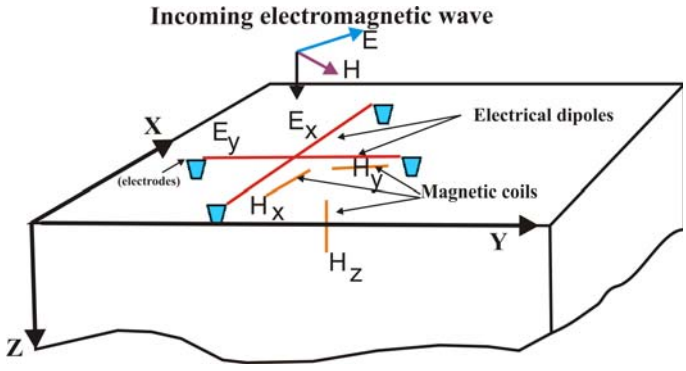

FIGURE 8: Field layout for a 5-channel MT data acquisition system

The depth of investigation using MT is much higher than that of other EM methods, which are usually unable to define geological features or detect geothermal reservoirs deeper than 1 km (Oskooi, 2006). Data acquisition at a single MT measurement point (Figure 8) is done by measuring the input fields, two horizontal magnetic components H_x and H_y, and the response from the earth, two horizontal electrical fields, E_x and E_y and a vertical magnetic field, H_z.

5.2 Homogenous earth

Cagniard (1953) and Keller and Frischknecht (1966) provide excellent introductions to the theory of magnetotelluric fields over a plane layered earth, which essentially is an outgrowth of concepts from the theory of the propagation of electromagnetic plane waves in a conductive medium that is linear, homogenous and isotropic. In such a medium, an electromagnetic wave propagates so that the electric

and magnetic field vectors are orthogonal. The ratio of electric to magnetic field intensity is a characteristic measure of the electromagnetic properties, often called the characteristic impedance, Z:

$$Z = \frac{\omega\mu_0}{k} = \frac{E_x}{H_y} = -\frac{E_y}{H_x} \quad (21)$$

where Z = Characteristic impedance (Ω);
ω = Angular frequency ($2\pi f$), where f is frequency (Hz);
μ_0 = Magnetic permeability (H/m);
E_{xy} = Electric field intensity (V/m) in x, y direction;
H_{xy} = Magnetic field intensity (A/m) in x, y direction;
k = $\sqrt{i\omega\mu(i\omega\varepsilon - \sigma)}$ stands for the wave propagation number;
σ = conductivity (S/m)
ε = Dielectric permittivity (C/Vm);

If displacement currents are neglected, k = $\sqrt{-i\omega\mu\sigma}$ and Equation 21 can be rewritten as:

$$Z = \frac{\omega\mu_0}{\sqrt{-i\mu_0\sigma\omega}} = \sqrt{i}\sqrt{\omega\mu_0\rho} = \sqrt{\omega\mu_0\rho}\; e^{i\pi/4} \quad (22)$$

and π/4 is phase difference between E_x and H_y (Figure 9). If the earth is homogenous and isotropic, then the true resistivity of the earth is related to the characteristic impedance through the relation: (Hermance, 1973)

$$\rho = 0.2T|Z|^2 = 0.2T\left|\frac{E_x}{H_y}\right|^2 \quad (23)$$

where ρ = Resistivity (Ωm);
T = Period (s).

And for a non-homogenous earth, apparent resistivity and phase are defined as:

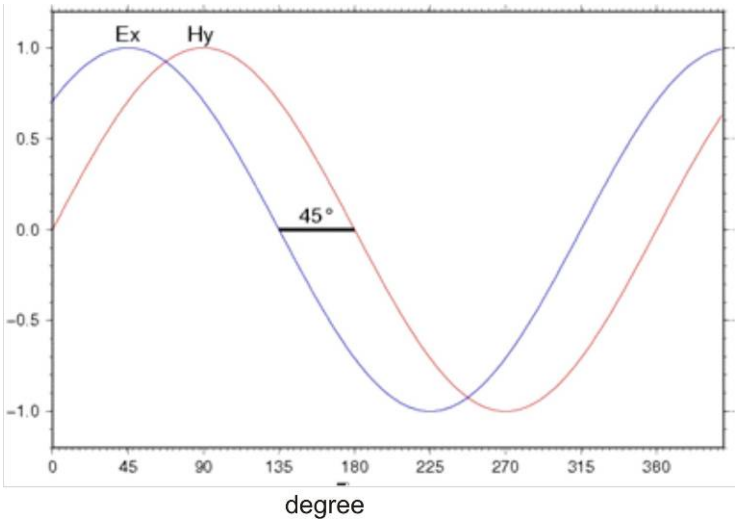

FIGURE 9: Homogenous half space response of electric and magnetic field

$$\rho_a = 0.2T|Z_0|^2 \; and \; \theta_a = arg(Z_0) \neq 45° \quad (24)$$

where Z_0 = Impedance at the surface.

An electromagnetic wave that propagates down into the conductive earth is attenuated. The skin effect δ (m) is the depth below the conductor surface at which the electromagnetic wave decreased to 1/e (approximately 37%) of its value at the surface. A useful approximation is given by:

$$\delta = \frac{1}{\mathrm{Re}(k)} = \frac{1}{\mathrm{Re}\,(\sqrt{-i\omega\mu\sigma})} = \sqrt{\frac{2}{\omega\mu\sigma}} = \sqrt{\frac{2T\rho}{2\pi\times4\pi\times10^{-7}}} = \frac{10^3}{\pi}\times\sqrt{\frac{20}{8}}\times\sqrt{T\rho} \approx 500\sqrt{T\rho} \quad (25)$$

where T = Time (s);
ρ = Resistivity (Ωm).

5.3 Layered earth

In the layers of a horizontally *N*-layered earth, the plane wave impedance is given by the recursive formula (Ward and Wannamaker, 1983) as:

$$\hat{Z}_N = \hat{Z}_N = \frac{\omega\mu}{k_N} \quad ; \qquad \hat{Z}_{n-1} = Z_{n-1}\,\frac{\hat{Z}_n + Z_{n-1}\,tanh(ik_{n-1}h_{n-1})}{Z_{n-1} + \hat{Z}_n\,tanh(ik_{n-1}h_{n-1})} \tag{26}$$

where Z_n $= \frac{\mu_0\omega}{k_n}$ (intrinsic impedance of the n[th] layer) with $k_n = \sqrt{-(i\omega\mu\sigma_n)}$;
h_n = Thickness of the n^{th} layer; and
$\hat{Z}_n$ = Impedance in the n^{th} layer; and
Z_1 = Z_0 is the impedance at the surface.

For a two layered model earth, of ρ_1, h and ρ_2, assuming that **E** = (E_x,0,0) and **H** = (0,H_y,0) (Figure 10), Equation 26 becomes:

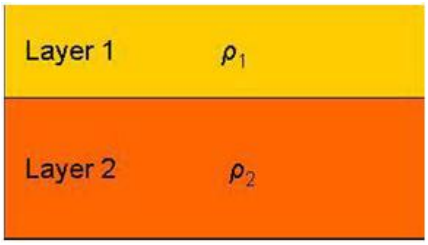

FIGURE 10: Two-layered earth

$$\hat{Z}_1 = Z_1\,\frac{\hat{Z}_2 + Z_1\tanh(k_1h)}{Z_1 + \hat{Z}_2 tah(k_1h)}; \text{ where } \quad k_1 = \sqrt{-(i\omega\mu/\rho)} = \sqrt{\frac{-i2\pi\mu}{\rho_1 T}} \tag{27}$$

For k_1h << 1, tanh (ik_1h) ≈ ik_1h for larger *T*, and then Equation 27 can be written as:

$$Z_0 = Z_1\left[\frac{\hat{Z}_2 + iZ_1k_1h}{Z_1 + i\hat{Z}_2k_1h}\right] = Z_1\left[\frac{Z_2 + iZ_1k_1h}{Z_1iZ_2k_1h}\right] \tag{28}$$

For $\rho_1 \gg \rho_2$, that means we have a conductor at depth h_1 and $Z_1 \gg \hat{Z}_2$. Then Equation 28 becomes:

$$Z_0 = Z_1\,[\frac{Z_2 + iZ_1\,k_1h_1}{Z_1 + iZ_2\,k_1h_1}] \;\approx\; iZ_1\,k_1h_1 = \frac{i\omega\mu}{k_1}\;k_1h_1 = i\omega\mu h_1, \tag{29}$$

and

$$\rho_a = \frac{1}{\omega\mu}|Z_0|^2 = \frac{1}{\omega\mu}(\omega\mu h_1)^2 = \frac{2\pi\mu {h_1}^2}{T} \tag{30}$$

Therefore the depth to the good conductor, h_1, can be calculated from ρ_a at longer periods, *T*, as:

$$h_1 = \sqrt{\frac{\rho_a T}{2\pi\mu}} \tag{31}$$

Equation 30 shows that the slope of $\log_{10}\rho_a$ vs. $\log_{10} T$ is always greater than -1.

For $\rho_1 \ll \rho_2$, that means we have an insulator at depth h_1 and $Z_1 \ll Z_2$. Then Equation 28 becomes:

$$Z_0 = Z_1\,[\frac{Z_2 + iZ_1\,k_1h_1}{Z_1 + iZ_2\,k_1h_1}] \;\approx\; Z_1\,\frac{1}{ik_1h_1} = \frac{\omega\mu}{ik_1{}^2}\,\frac{1}{h_1} = \frac{1}{\sigma_1h_1}\,\frac{1}{S} \tag{32}$$

where S = Conductance of the of layer 1; and

$$\rho_a = \frac{1}{\omega\mu}|Z_0|^2 = \frac{1}{\omega\mu}\frac{1}{S^2} = \frac{T}{2\pi\mu}\,\frac{1}{S^2} \tag{33}$$

Therefore, the conductance of layer 1 can be calculated from ρ_a at longer periods, *T*, as:

$$S = \sqrt{\frac{T}{2\pi\mu\rho_a}} \tag{34}$$

Equation 33 shows that the slop of $\log_{10}\rho_a$ vs. $\log_{10} T$ is always less than 1.

5.4 Static shift

Surficial bodies can severely distort magnetotelluric (MT) apparent resistivity data to arbitrarily low frequencies. This galvanic distortion effect, known as the MT static shift, is due to an electric field generated from boundary charges on surficial inhomogeneities, and persists throughout the entire MT recording stage. Static shifts are manifested in the data as vertical, parallel shifts of log-log apparent resistivity sounding curves, the impedance phase being unaffected.

Using central-loop TEM data acquired at the same location provides a natural remedy for the MT static shift. This is because TEM is less sensitive to lateral resistivity variations as it records the secondary magnetic field, and the magnetic field is not affected by charge accumulation at boundaries of shallow heterogeneities. The MT sounding curve is shifted vertically so that the high frequency part of the MT curve agrees with the TEM curve. The low frequency MT curves then provide an undistorted picture of the deep resistivity section (Jones, 1988; Pellegrin and Hohmann, 1990).

6. INTEGRATED TEM AND MT SURVEY AT THE HENGILL AREA

The Hellisheidi geothermal system (Franzson et al., 2005), the study area, is located in the southwest part of the Hengill central volcano. The prospect area is in the southwest extension of the Hengill fissure swarm (Figures 11 and 12). The geothermal area within the Hengill volcanic system is referred to as the Hengill geothermal area. Hellisheidi is one of the three main well fields in the Hengill area, i.e. Nesjavellir, Hellisheidi and Hveragerdi fields. The purpose of this TEM and MT integrated study was to get detailed picture of the resistivity structure of the area, and to see if the trend of the geothermal system agrees with the fissure swarm as seen on the surface. In an earlier survey, an indication of the existence of a resistivity structure corresponding to a high-temperature geothermal field was found in the southwest part of the Hengill area (Árnason, 2006a).

6.1 Geology of Hengill area

The Mid-Atlantic Ridge, the constructive boundaries between the North American and Eurasian plates, crosses Iceland from southwest to northeast. This boundary in Iceland is characterized by a zone of rifting and volcanic activities (Flóvenz et al., 1985). The Hengill area, which is entirely made up of volcanic rocks, hyaloclastite formations and basaltic fissure lavas produced in an active fissure swarm, is situated within the rift system. Investigation of the Hengill volcanic complex indicates that super critical conditions are found at a shallow depth, ~5 km, and perhaps at less than 3 km depth associated with the youngest volcanic structure in the western part of the Nesjavellir geothermal system in the northeast part of the Hengill area (Fridleifsson et al., 2003).

There are two main volcanic fissures of Holocene age and trending NE-SW in the Hengill area, that have fed the last volcanic eruptions in the area, extending from Lake Thingvallavatn in the northeast part of the Hengill area (Nesjavellir high-temperature field) about 20 km to the southwest of the Hengill mountain (Hellisheidi geothermal field) (Saemundsson, 1995). The age of the older fissure is about 5500 years and the younger one is about 2000 years old (Saemundsson, 1967). The lava flows are widespread and cover a large part of the Hellisheidi area. These eruptive fissures and parallel faults control up- and out-flow of hot water and steam from the centre of the Hengill system. Tectonic

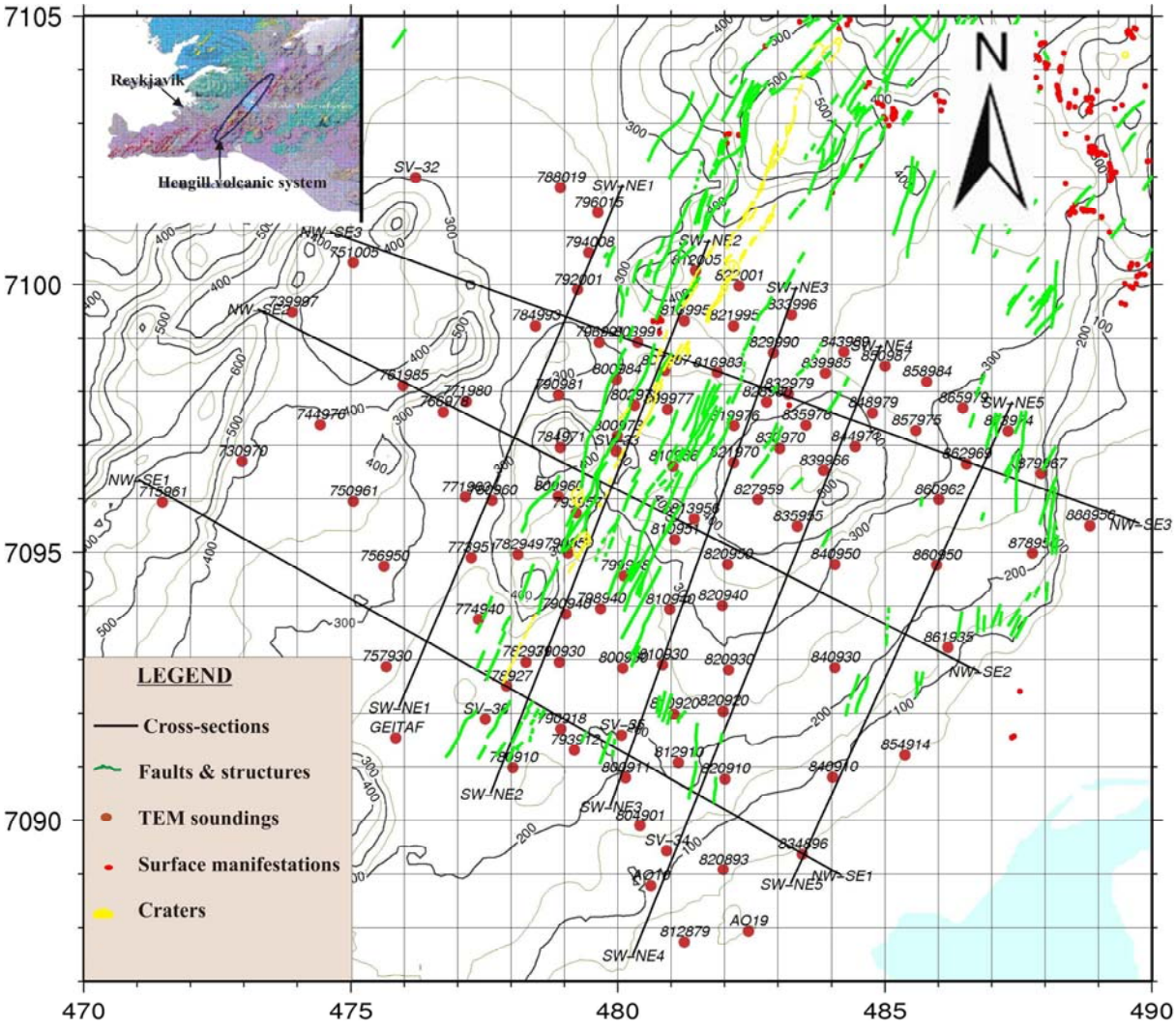

FIGURE 11: Location map of TEM soundings and cross-sections

activity is episodic and accompanied by rifting and major faulting along the fissure swarm that intersects the Hengill central volcano, and by magma being injected into the fissure swarm. A row of small craters is marked along both the older and younger eruptive fissures.

6.2 TEM survey and equipment

To properly learn how to collect TEM data, a TEM survey was carried out in collaboration with a field crew from Iceland Geo-survey (ÍSOR). For the TEM resistivity survey, the Time Domain Electro Magnetics PROTEM digital receiver and a TEM-67 transmitter of Geonics Ltd. were used. For the purpose of this project work, a total of 106 TEM soundings (previously collected data) were processed (Figure 11).

The sounding data were collected using single turn transmitter wire loop of 300 × 300 m, covering an area of 90,000 m^2. Two receiver loops were used, a small coil with an effective area of 100 m^2, and a flexible loop with an effective area ranging from ~4000 m^2 to ~8000 m^2. The transmitted current was usually in the range of 18-22 A, transmitted at a high frequency of 25 Hz, and a low frequency of 2.5 Hz. For each frequency, 20 measuring time gates were evenly spaced on a log-scale from 0.09 to 7 ms for the high frequency and 0.9 to 70 ms for the low frequency after current turn off. Repeated transients were stacked and stored in the computer memory of the receiver and later downloaded to a personal computer ready for further processing.

6.3 TEM data processing and interpretation

The TEMX program was used to read raw data files downloaded from the PROTEM-D3 receiver. TEMX program calculates averages and standard deviations for repeated transient voltage measurements and calculates late time apparent resistivity as a function of time. The program also offers rejecting noisy readings through graphical-user interface (GUI).

An interpretation program called TEMTD (Árnason, 2006b) was used to perform the 1D layered-earth inversion on the data (see examples of data curves in Appendix I). The program assumes that the source loop is a square loop and that the receiver coil/loop is at the centre of the source loop. The current wave form is assumed to be a half-duty bipolar semi-square wave with exponential current turn-on and linear current turn-off. The program also uses the GNUPLOT graphics program for graphical display during the inversion process.

The inversion algorithm used in the program is the nonlinear least-squares inversion of the Levenberg-Marquardet type (Árnason, 1989). The misfit function is the root-mean-square difference between measured and calculated values (*chisq*), weighted by the standard deviation of the measured values. The user is offered the option of choosing whether the program fits the measured voltage or the late time resistivity values.

The program offers the possibility of keeping models smooth, both with respect to resistivity variations between layers (logarithm of conductivities) and layer thickness (logarithm of ratio of depth to top and bottom of layers). The damping can be done both on first derivatives which counteracts sharp steps in the model, and on the second derivatives which counteracts oscillations in the model values. The actual function that is minimised is not just the weighted root-mean-square misfit, *chisq*, but the potential:

$$Pot = chisq + \alpha * DS1 + \beta * DS2 + \gamma * DD1 + \delta * DD2 \quad (35)$$

*DS*1 and *DS*2 are the first and second order derivatives of log conductivities in the layered model, and *DD*1 and *DD*2 are the first and second order derivatives of the logarithms of the ratios of layer depths. The coefficients α, β, γ and δ are the relative contributions of the different damping terms.

The program is also used to perform minimum structure (Occam´s) inversion; in this case the layer thickness are kept fixed, equally spaced on a log scale, and the conductivity distribution is forced to be smooth by adjusting α and β in Equation 35 (damping of layer thickness is ignored in this case; the number of layers are 20-40).

6.4 MT survey and equipment

Similar to that of TEM, MT data was collected in collaboration with a field crew of Iceland Geo-survey (ÍSOR) to learn the collecting procedures, while the MT sounding data used for interpretation in this project were collected in the summer 2006 from the Hengill area, within the same area where TEM sounding data were collected. A 5-channel MT data acquisition system (MTU-5A) from Phoenix Geophysics Canada was used. The field layout is given in Figure 8. For this project work, EDI files (47 soundings), processed from the time series data (see below) were given for interpretation (Figure 12).

6.5 MT data processing and interpretation

For practicing purposes, time-series data downloaded from the MTU-5A units were viewed using the program Synchro Time Series View. This program allows viewing and printing of graphical

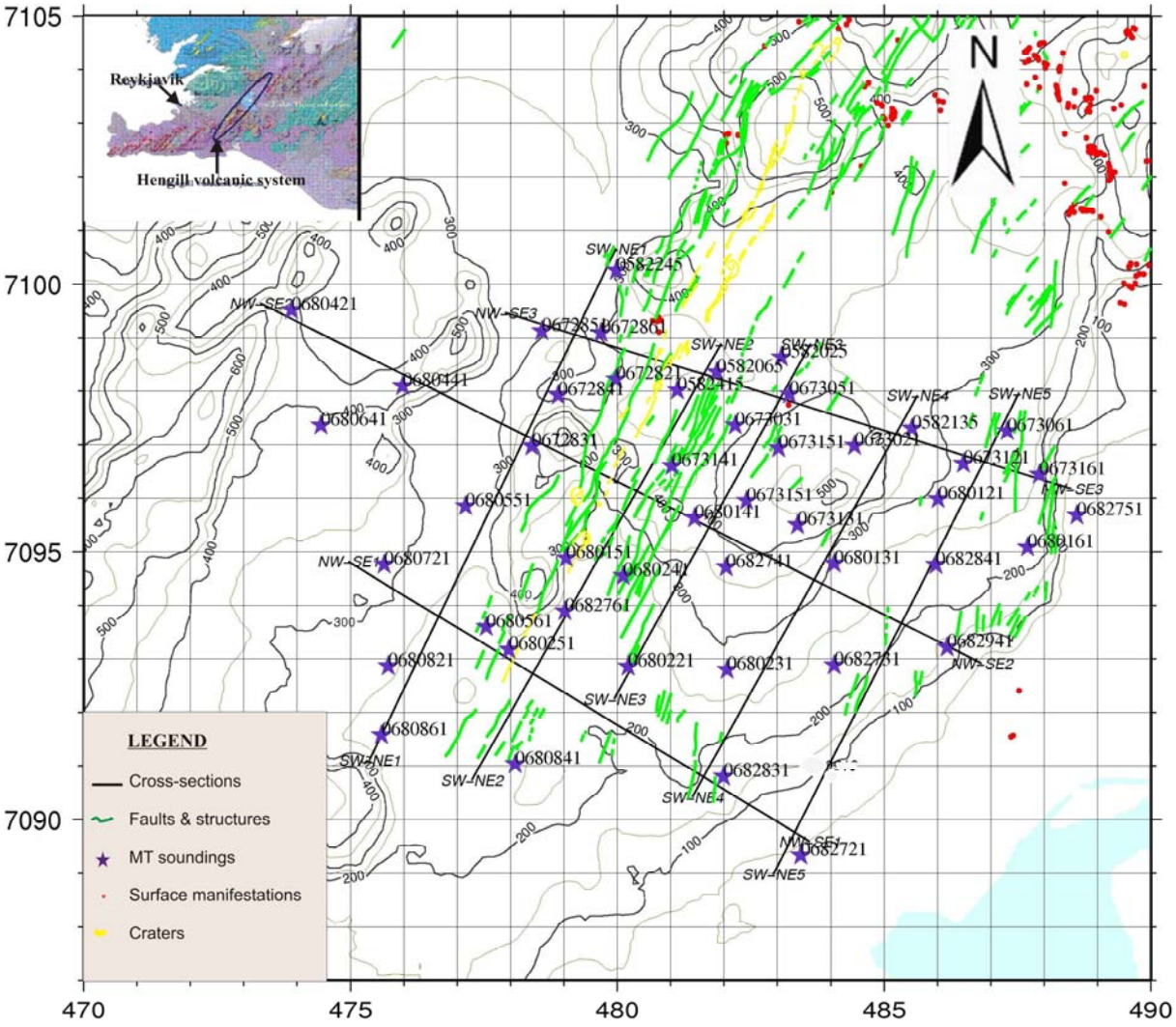

FIGURE 12: Location map of MT soundings and cross-sections

representations of the raw time-series data, power spectra derived from the time-series data and coherence between pairs of orthogonal channels. Using the program SSMT2000, provided by Phoenix Geophysics-Canada (Phoenix Geophysics, 2005), Fourier transforms were produced from the raw time-series data. Fourier coefficients were then reprocessed using data from the reference site to filter out noise-affected data. The cross-powers were stored in files and could be displayed graphically using the MTU-Editor program. Those files were then converted to industry-standard EDI format for use with geophysical interpretation software (in this case, TEMTD).

For this project work, EDI files were given and inverted with the program TEMTD (similar to that of TEM data, as mentioned in Section 6.3). In this study, rotational invariant apparent resistivity and phase were inverted to a layered model. TEM data from the same area were jointly inverted with the MT data; in this case TEMTD determined the best static shift parameter for the MT data. Static shift of these data sets ranges from 0.5 to 1.3, the majority being around 0.8 (see examples of jointly inverted curves in Appendix II).

7. RESULTS

Aiming at defining the boundary of the Hellisheidi high-temperature geothermal system in the Hengill area, 1D inversions of the TEM and MT soundings (Occam files) were made using the TEMTD program. The results were used to create iso-resistivity maps and cross-sections with the help of the programs TEMRESD and TEMCROSS, written by Dr. Hjálmar Eysteinsson (2007), and based on the GMT program package.

A resistivity structure of a high-temperature field is usually characterized by unaltered fresh rock at the surface and a low-resistivity cap or layer underlain by a high-resistivity core. This situation can also be related to temperature, provided equilibrium exists between the resistivity and temperature, as discussed in Section 3.4.

7.1 TEM resistivity maps

Iso-resistivity maps show the resistivity distribution at depth. TEM iso-resistivity maps at 100 m a.s.l., sea level, and 300, 500, 700 and 900 m b.s.l. are presented in Figures 13-18. The iso-resistivity maps at 100 m a.s.l. and at sea level (Figures 13 and 14) show a dominant high-resistivity layer, associated with the fresh and unaltered, near-surface rock in most parts of the area. At the same depths, a low-resistivity body is also depicted along the fissure swarm trending NE-SW. This low resistivity is due to alteration of the formation with in the fissure swarm due to higher temperatures associated with hot fluids flowing up or along the fissures. At these shallow depths, the high resistivity in the near-surface formations is more pronounced in the western part of the area.

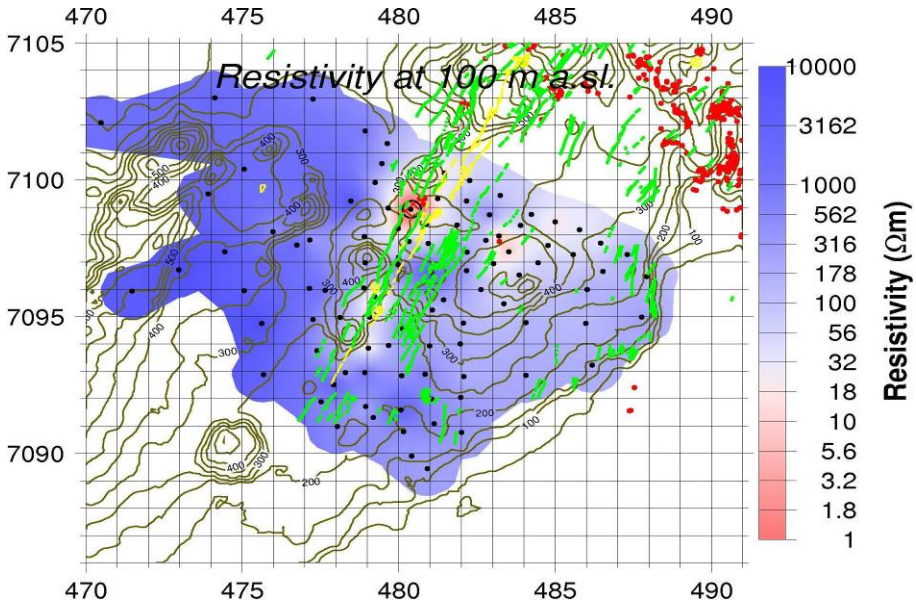

FIGURE 13: TEM resistivity distribution at 100 m a.s.l

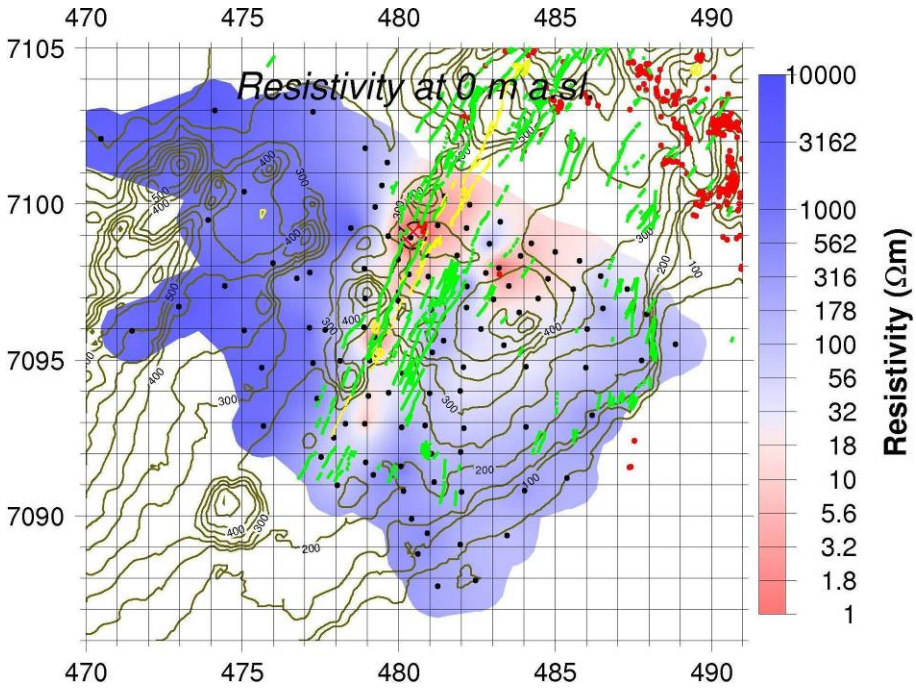

FIGURE 14: TEM resistivity distribution at sea level

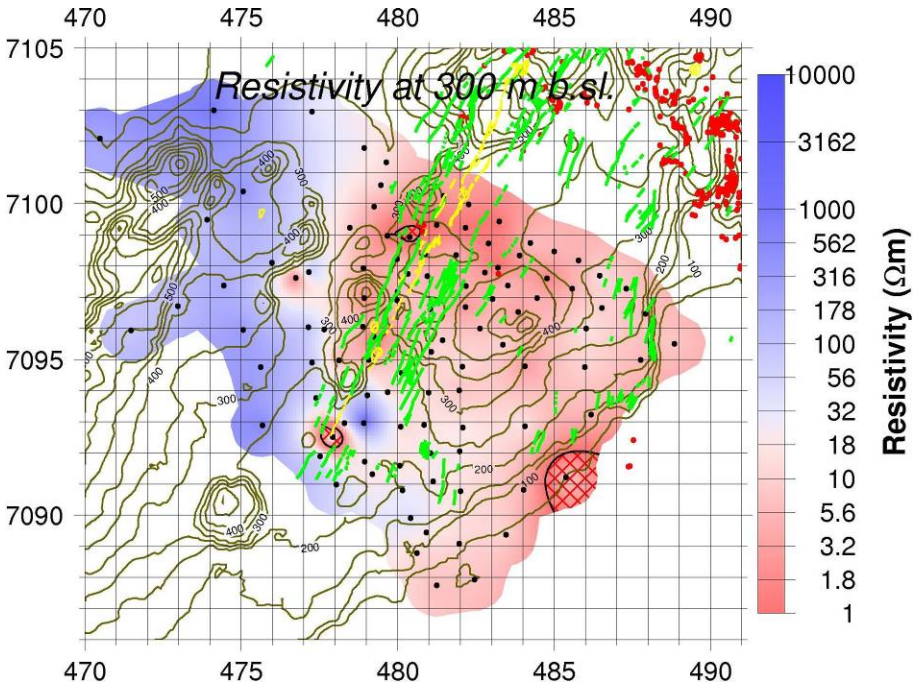

FIGURE 15: TEM resistivity distribution at 300 m b.s.l.

The iso-resistivity maps in Figures 15-18 show the resistivity structure at depths of 300-900 m b.s.l. At 300 m b.s.l. (Figure 15) the higher-resistivity near-surface formation is still prominent in the western part, but elsewhere and at deeper levels, these maps show a low resistivity distributed over basically the whole area. Moreover, a high resistivity (in red/dark hash lines) is seen below the low-resistivity layer. This high-resistivity core is first seen at 300 m b.s.l., and appears there in small patches, mainly within the central part of the fissure swarm trending NNE-SSW. At deeper levels (Figures 17 and 18) it grows in size, especially in the southern part of the area.

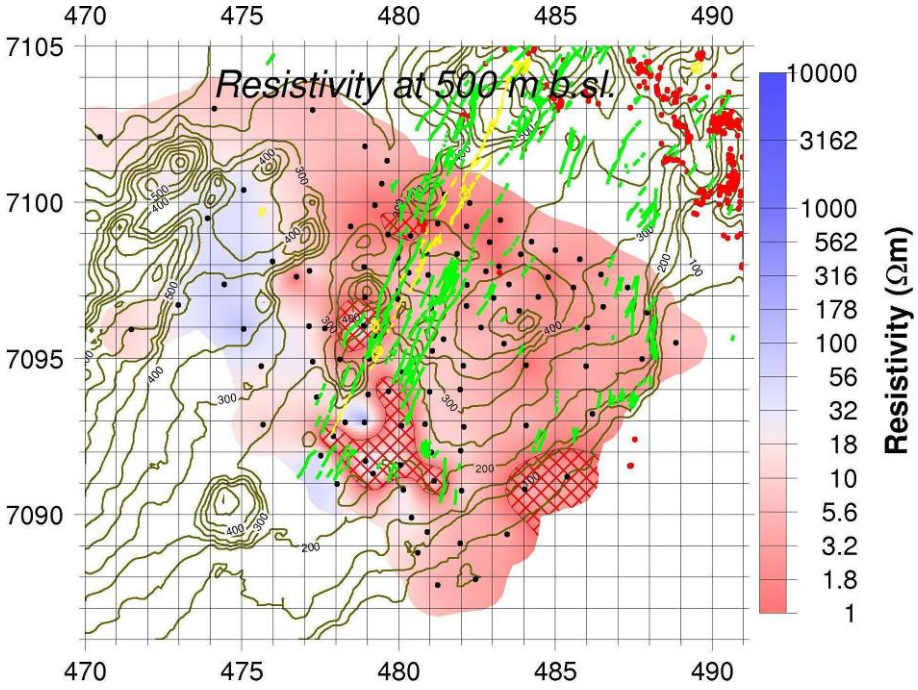

FIGURE 16: TEM resistivity distribution at 500 m b.s.l.

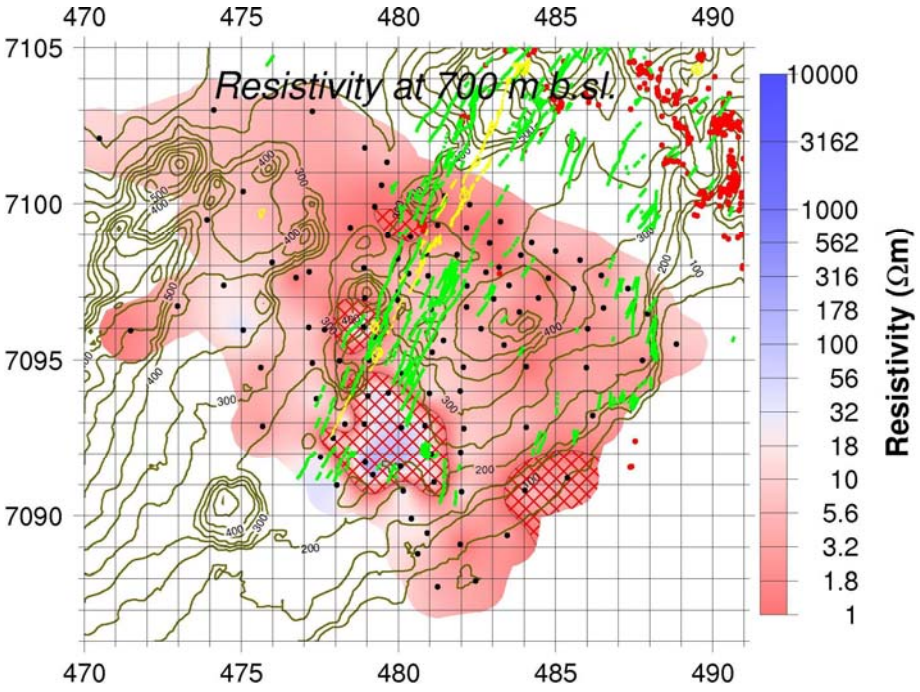

FIGURE 17: TEM resistivity distribution at 700 m b.s.l.

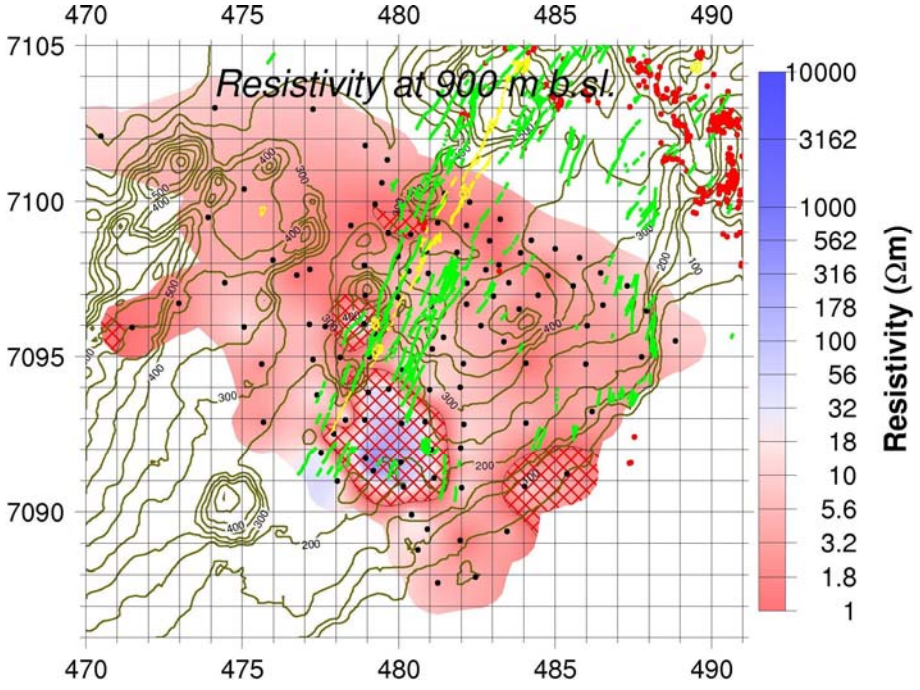

FIGURE 18: TEM resistivity distribution at 900 m b.s.l.

7.2 TEM cross-sections

Seven TEM resistivity cross-sections from Hellisheidi geothermal field are presented here. Four of them are SW-NE trending (SW-NE1, SW-NE2, SW-NE3 and SW-NE5), along or parallel to the fissure swarm (Figures 19-22), and three of them are trending NW-SE, across the fissure swarm (Figures 23-25). The locations of these cross-sections are shown on Figure 11.

Cross-section SW-NE1 (Figure 19) passes parallel to the western margin of the fissure swarm. It cuts high resistivity, the near-surface unaltered fresh rock formation right from the surface down to 300-

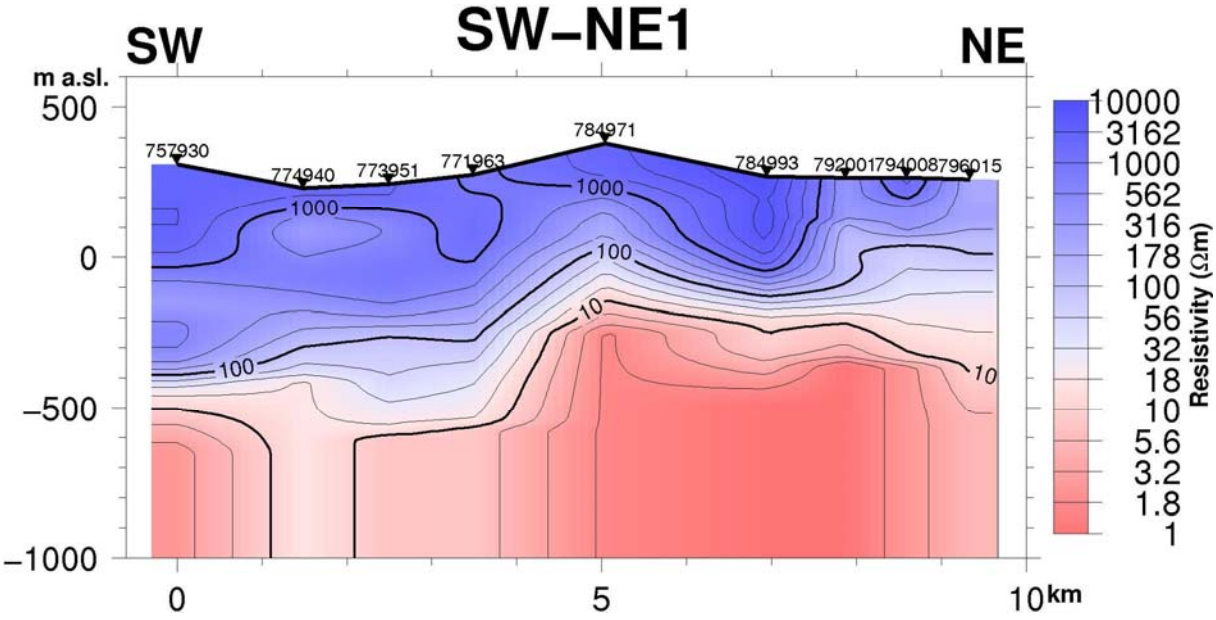

FIGURE 19: TEM cross-section SW-NE1

400 m b.s.l. Below, low-resistivity formations are seen. This low resistivity is probably associated with the clay alteration mineralogy all along the length of the profile.

Resistivity cross-section SW-NE2 (Figure 20) shows a high-resistivity core below a low-resistivity cap along 6 km length, appearing at about 500 m b.s.l. This high-resistivity core is relatively deep (at about 600 m b.s.l.) under soundings 790930 and 790940. In the north-eastern part, the low-resistivity formation is seen along the profile, with its top part reaching close to sea level. A low-resistivity layer is also observed to intercalate the near-surface high-resistivity formations at about sea level under soundings 790930 and 790940; this intercalation of low resistivity could be due to lateral flow of hot fluid along some fractures.

Resistivity cross-section SW-NE3 (Figure 21) cuts the high-resistivity core below a thin layer of a low-resistivity cap in the southern part of the section. The high resistivity is seen at about 600 m b.s.l., with its top reaching about 350 m b.s.l. below sounding SV-35. The length of the high-resistivity core is about 3 km but, due to lack of data, the southern boundary of the anomaly is not seen. The rest of

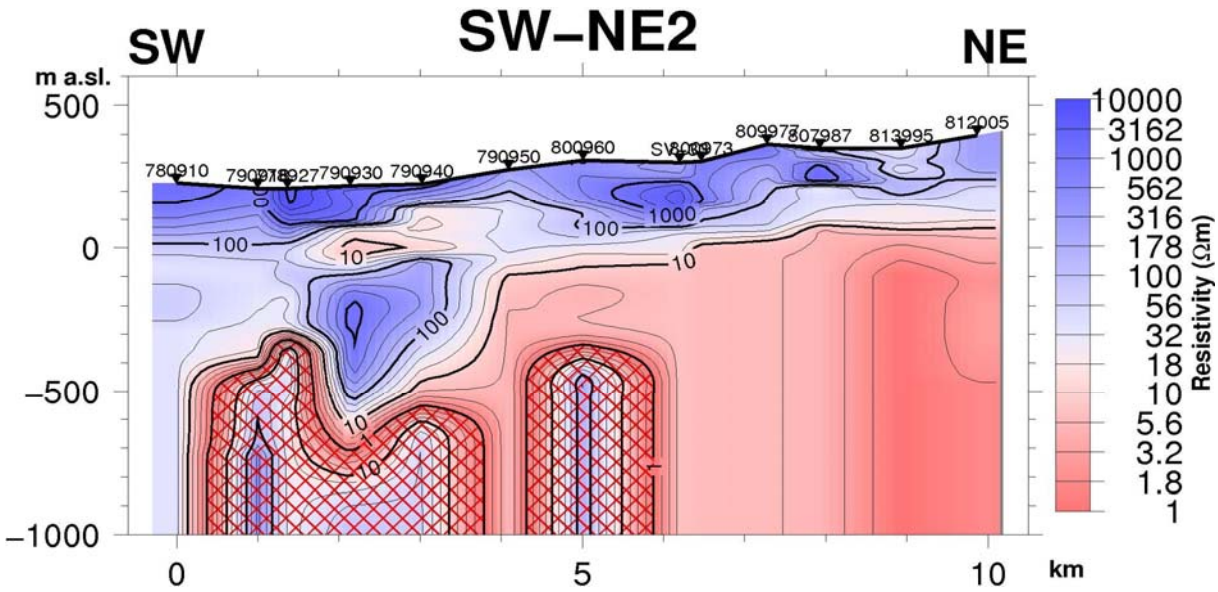

FIGURE 20: TEM cross-section SW-NE2

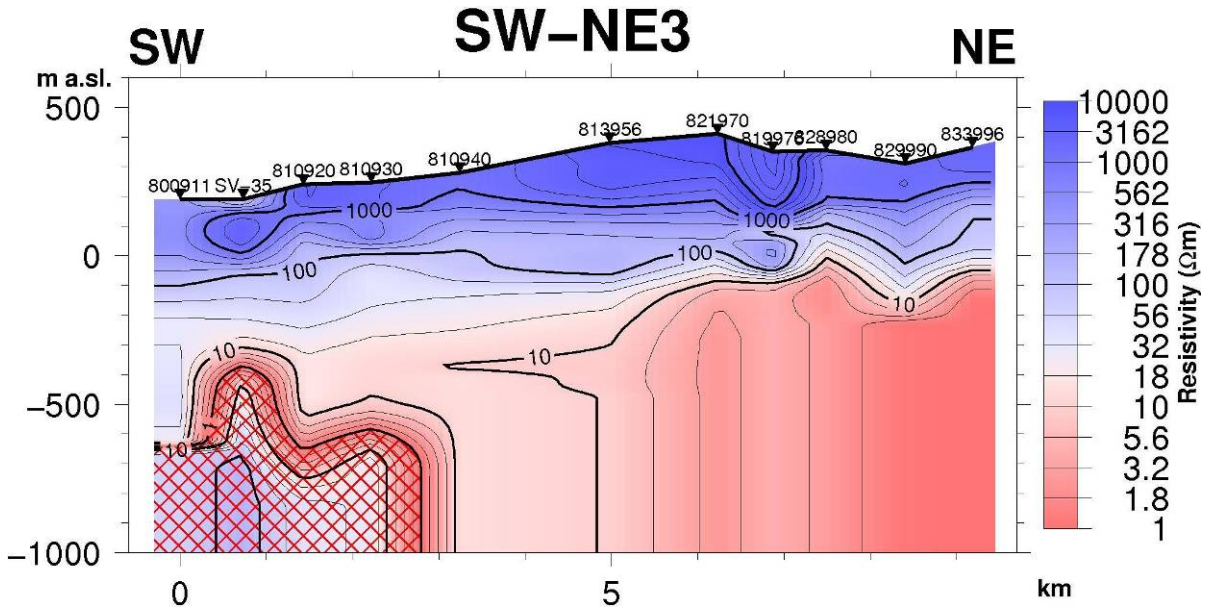

FIGURE 21: TEM cross-section SE-NE3

the cross-section, towards northeast, shows only the low-resistivity formation below the fresh unaltered volcanic rocks.

Resistivity cross-section SW-NE5 (Figure 22) is quite similar. It cuts a high-resistivity core below a low-resistivity cap at about 400 m b.s.l., but the difference between the resistivity values of the low-resistivity layer above and those of the high-resistivity core is less.

Resistivity cross-sections NW-SE1, NW-SE2 and NW-SE3, presented in Figures 23-25, describe the resistivity structure across the fissure swarm. Cross-section NW-SE1 (Figure 23) shows a highly resistive formation from the surface down to 400 m b.s.l., with lower resistivity at deeper levels on its western side. In the central part it cuts the high-resistivity core below a low-resistivity cap at about 400 m b.s.l. On the eastern side, the near surface high-resistivity layer is much thinner. The other two NW-SE trending cross-sections (Figures 24 and 25) are similar, but show a narrower high-resistivity core, about 2 km in width. This indicates that at this depth the geothermal reservoir, associated with

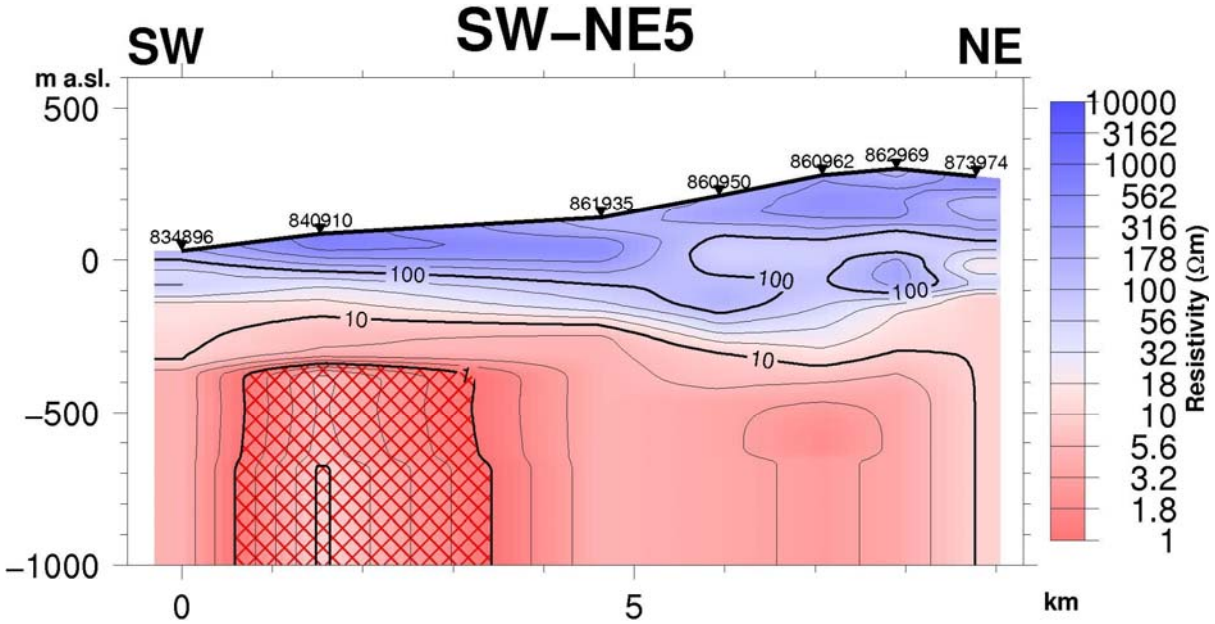

FIGURE 22: TEM cross-section SE-NE5

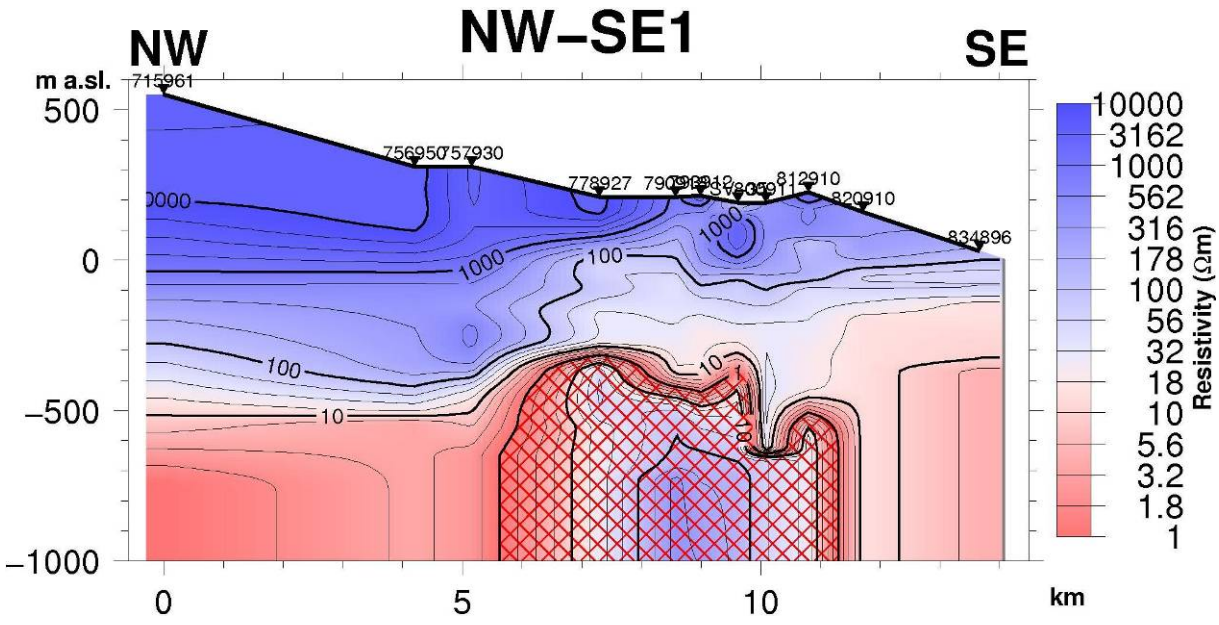

FIGURE 23: TEM cross-section NW-SE1

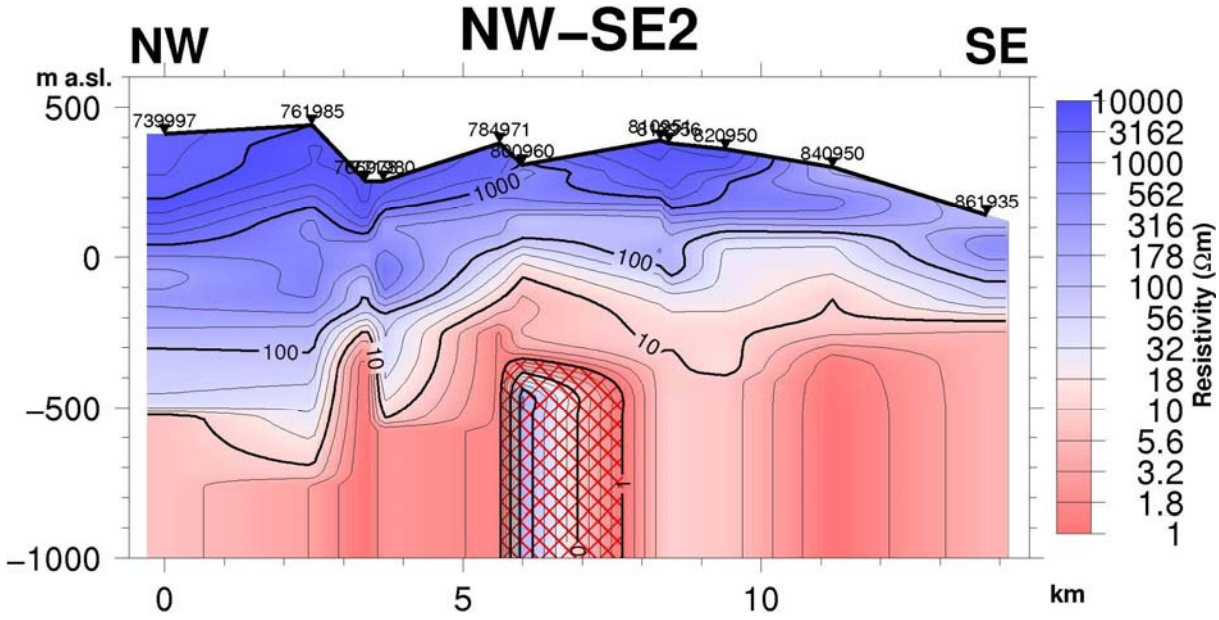

FIGURE 24: TEM cross-section NW-SE2

the high-resistivity core, is relatively narrow across the fissure swarm. Resistivity cross-section NW-SE3 shows the high-resistivity core reaching close to the surface within the fissure swarm, directly below sounding 803991; where the top part of the low-resistivity cap above also reaches to the surface.

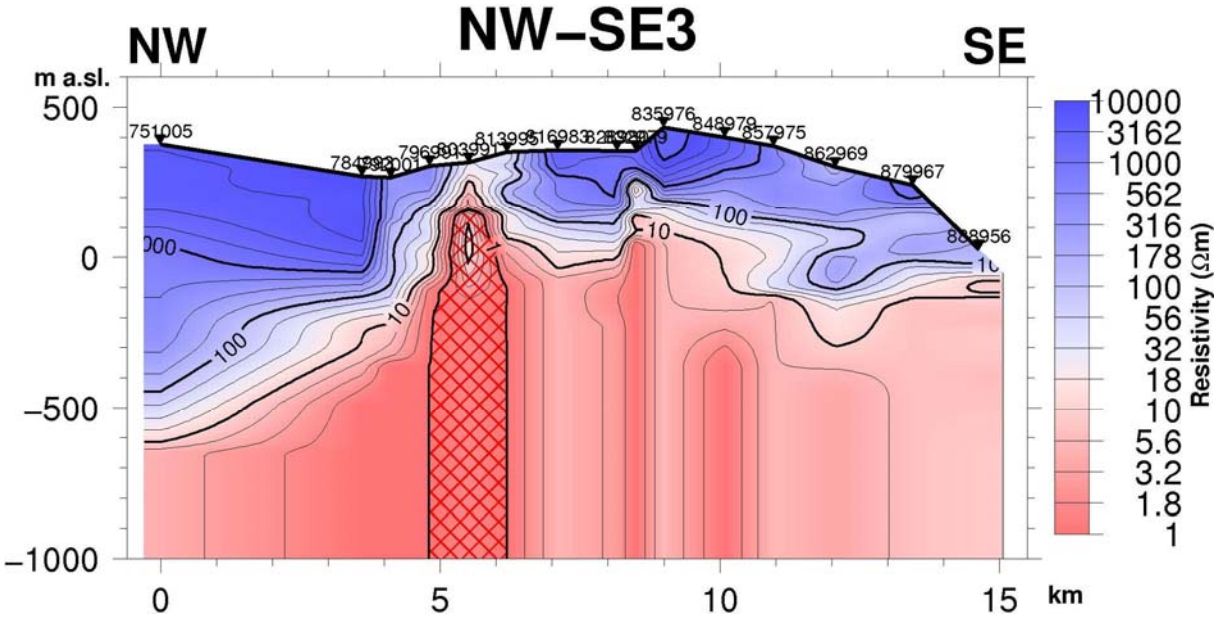

FIGURE 25: TEM cross-section NW-SE3

7.3 MT iso-maps

MT iso-resistivity maps at 500, 2000, 5000, 8000 and 15000 m b.s.l. are shown in Figures 26-30. The MT resistivity distribution down to about 900 m b.s.l. is similar to that of the TEM resistivity distribution. The MT resistivity distribution at 500 m b.s.l. is (Figure 26) presented for comparison with the TEM resistivity distribution presented in Figure 16. The MT map depicts a relatively low resistivity (1-20 Ωm) in almost the whole area, except in the western part which has a relatively higher resistivity, ranging from 32 to 178 Ωm. With less data density, the details are not the same as in the TEM map.

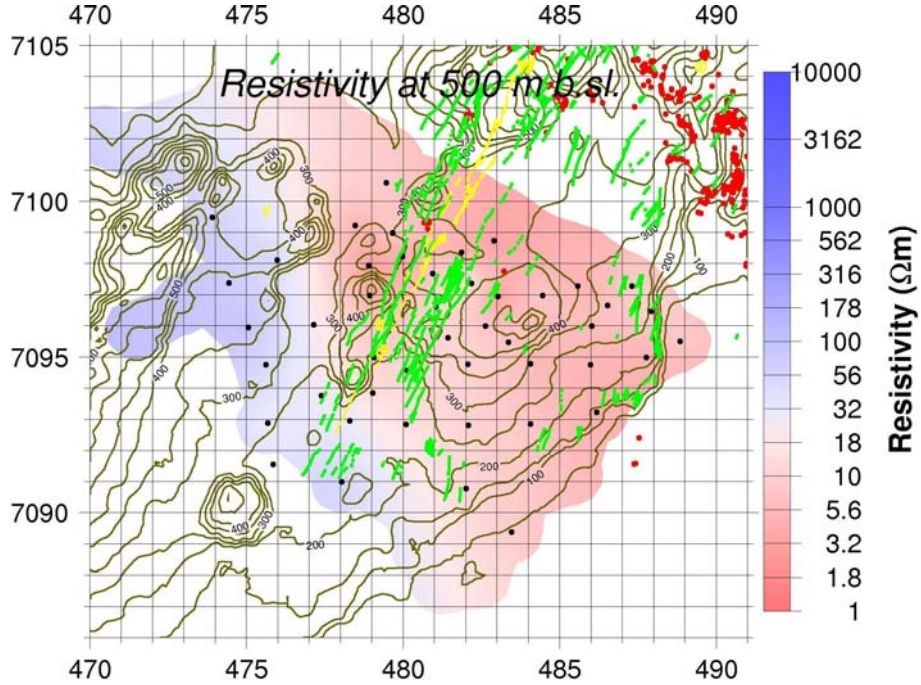

FIGURE 26: MT resistivity distribution at 500 m b.s.l.

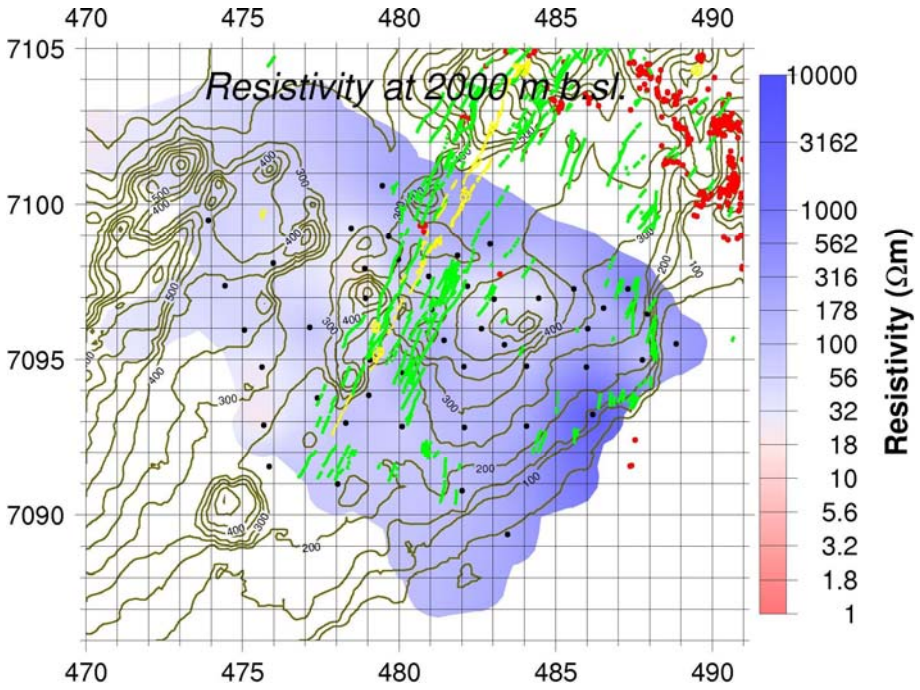

FIGURE 27: MT resistivity distribution at 2000 m b.s.l.

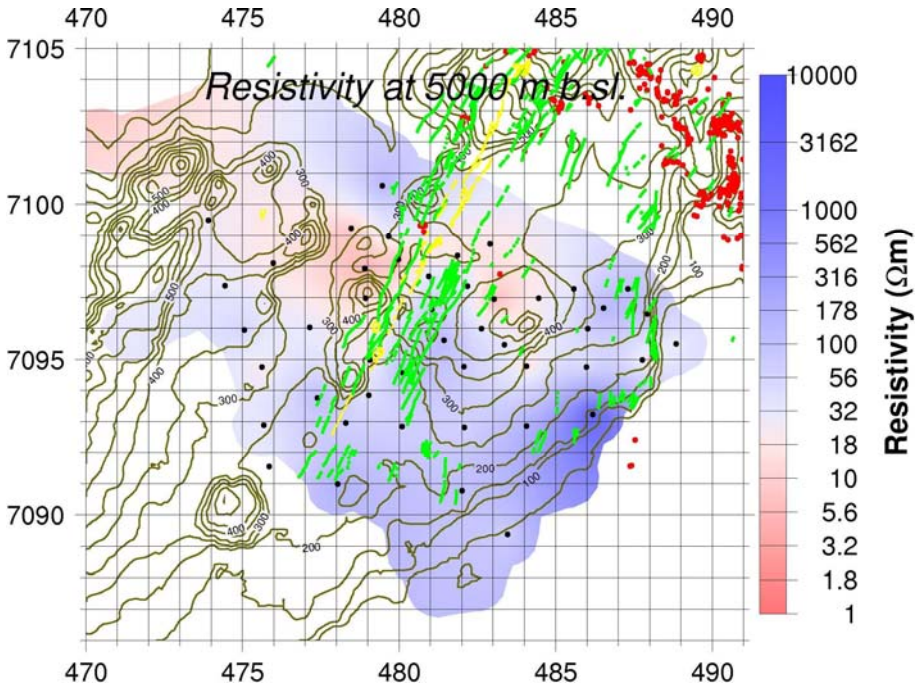

FIGURE 28: MT resistivity distribution at 5000 m b.s.l.

The MT iso-resistivity map at 2000 m b.s.l. (Figure 27) shows higher resistivity values with few spots of low resistivity. This higher resistivity distribution should represent the distribution of the chlorite and chlorite-epidote alteration zone.

The iso-map at 5000 m b.s.l. (Figure 28) shows higher resistivity in the southern and eastern parts but a lower resistivity in the northern part. The iso-resistivity map at 8000 m b.s.l. (Figure 29) shows widely distributed low resistivity. This low resistivity could represent a layer of high temperature that probably could be associated with cooling magma intrusions, the heat source for the high-temperature geothermal system discussed above. The MT iso-resistivity map at 15,000 m b.s.l. (Figure 30) shows again higher resistivity values approximately ranging from 56 to 316 Ωm.

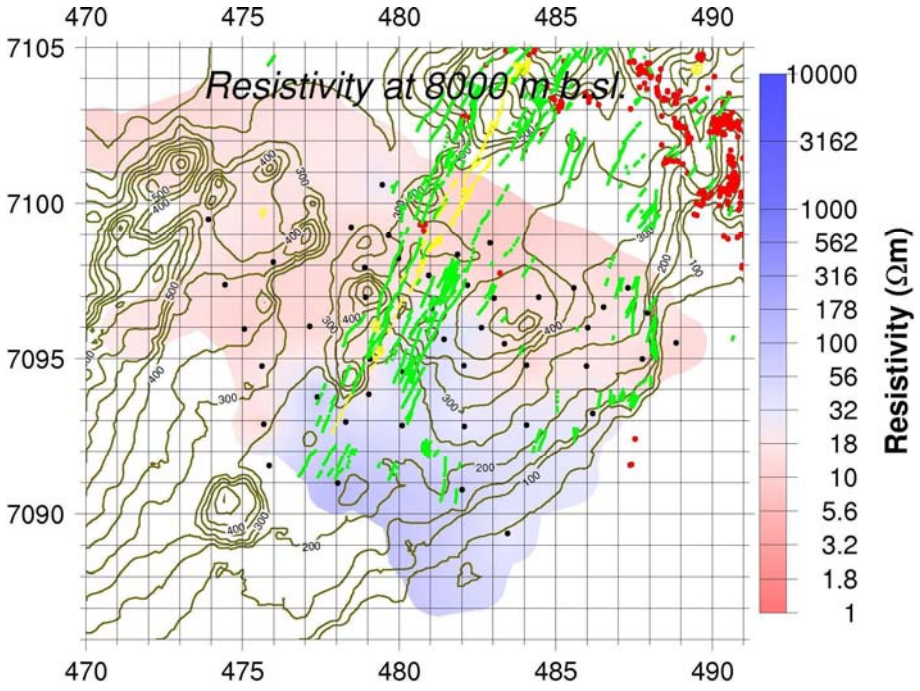

FIGURE 29: MT resistivity distribution at 8000 m b.s.l.

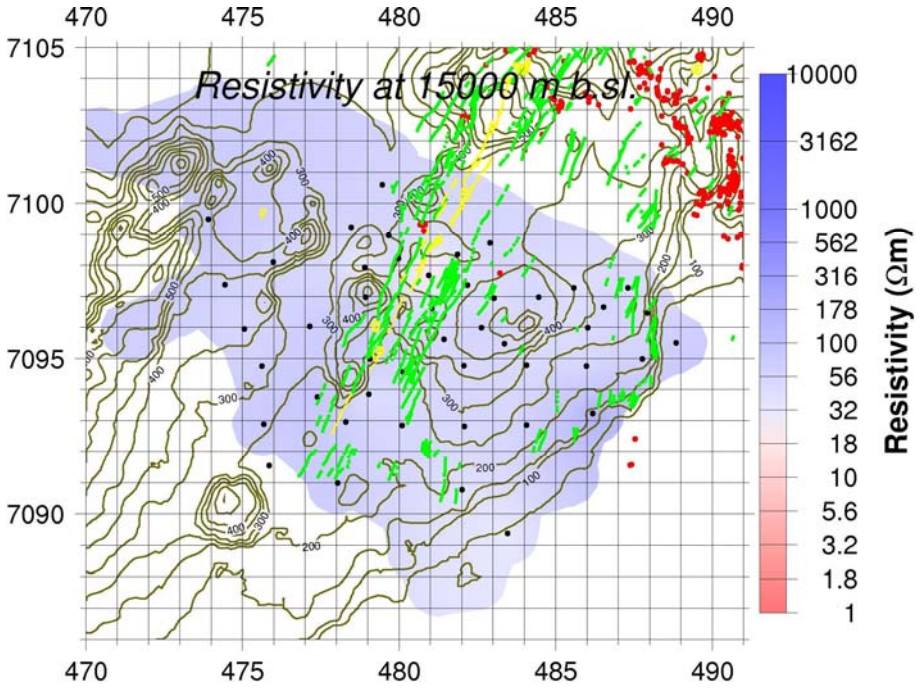

FIGURE 30: MT resistivity distribution at 15,000 m b.s.l.

7.4 MT cross-sections

Seven MT cross-sections are presented here. Four of them, SW-NE1, SW-NE2, SW-NE4 and SW-NE5 (Figures 31-34) pass parallel to the fissure swarm while the other three, NW-SE1 and NW-SE2 and NW-SE3 (Figures 35-37) are perpendicular to the fissure swarm. The location of these MT cross-sections is shown in Figure 12.

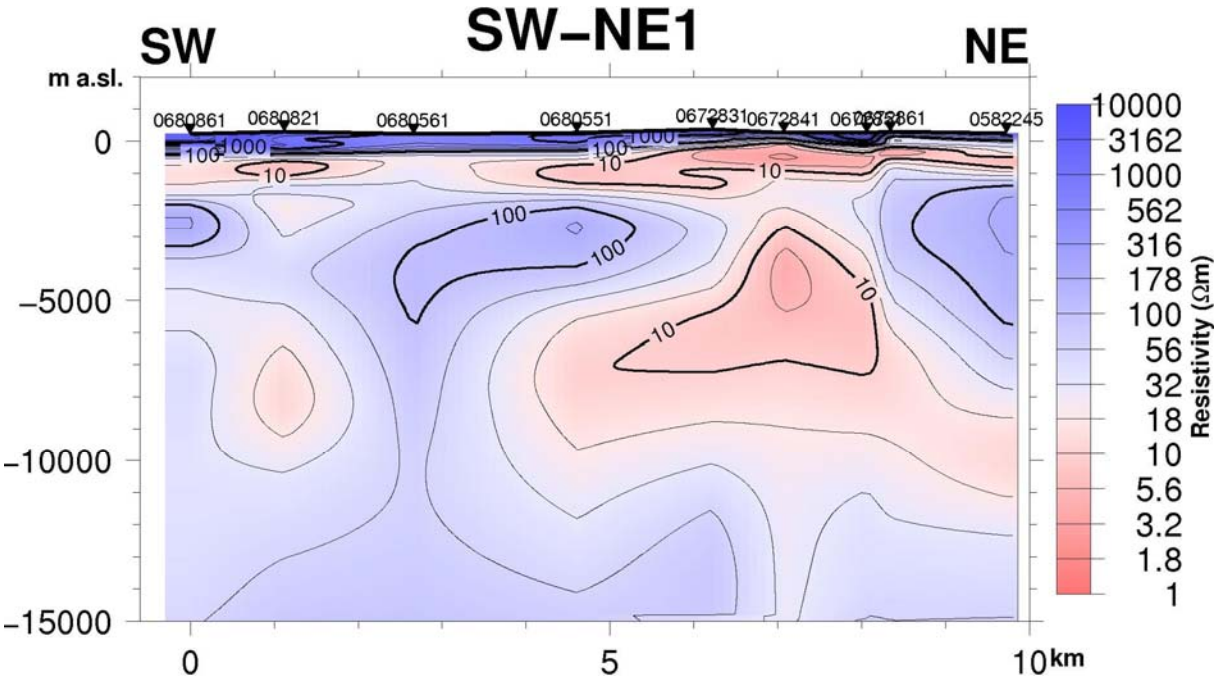

FIGURE 31: MT resistivitv cross-section SW-NE1

All the MT cross-sections cut through two low-resistivity formations, between approximately 500 and 1000 m b.s.l., and at about 5000-10000 m b.s.l., along almost the whole profile in most of the cross-sections. The upper low-resistivity layer is the traditional low-resistivity layer associated with low-temperature alteration, while the reason for the lower one is not clear. It could be related to partially molten basaltic magma layer or magmatic brine. These MT cross-sections are similar to the TEM cross-sections down to about 1000 m b.s.l., although they may look different due to the different scales of the cross-sections. To emphasize the similarity of the cross-sections, a detailed example of the MT resistivity distribution in cross-section SW-NE1 down to 1000 m b.s.l. is presented in Figure 38, showing very similar resistivity distribution as in the TEM cross-section in Figure 19.

MT cross-section SW-NE1 (Figure 31), which passes parallel to the fissure swarm on its western

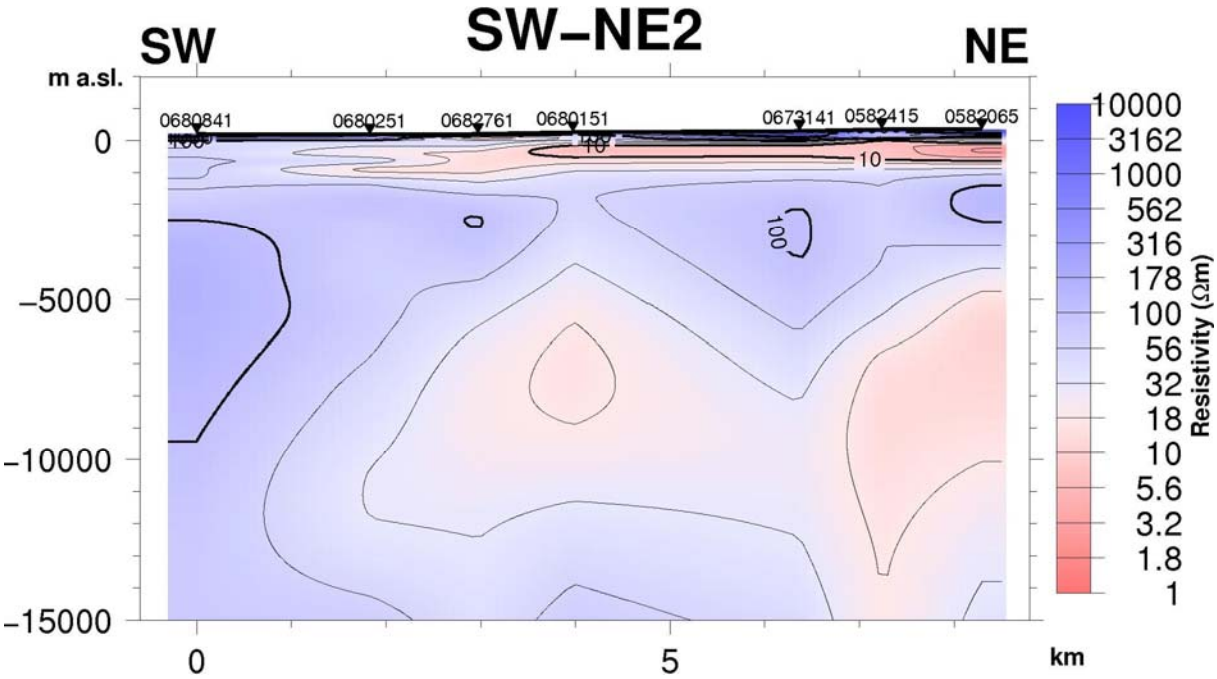

FIGURE 32: MT resistivity cross-section SW-NE2

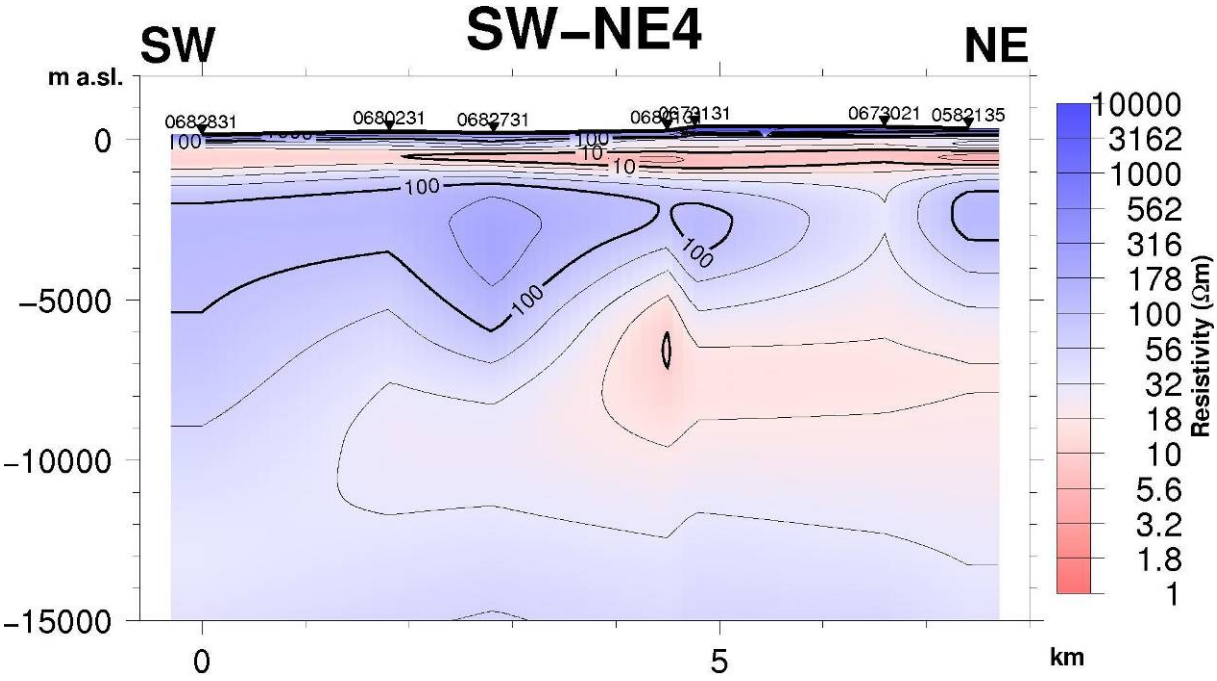

FIGURE 33: MT resistivity cross-section SW-NE4

margin, shows two low-resistivity bodies at about 5 km depth under the middle and the northeast part of the profile.

MT cross-sections SW-NE2 and SW-NE4 (Figures 32-33) show similar resistivity distribution in that they show a low-resistivity layer at about 300-900 m b.s.l. along the whole profiles. In addition, MT cross-section SW-NE4, which is located along the main fissure swarm, shows the lower low-resistivity layer (approximately 1 km wide) to stretch downward to below 15,000 m b.s.l.

MT cross-section SW-NE5 (Figure 34), which passes through the eastern side of the study area, shows a prominent high-resistivity body in its central part, between the low-resistivity layers. The highest resistivity (> 10,000 Ωm) is observed directly below sounding 0682941, in the depth range 2000-5000 m b.s.l.

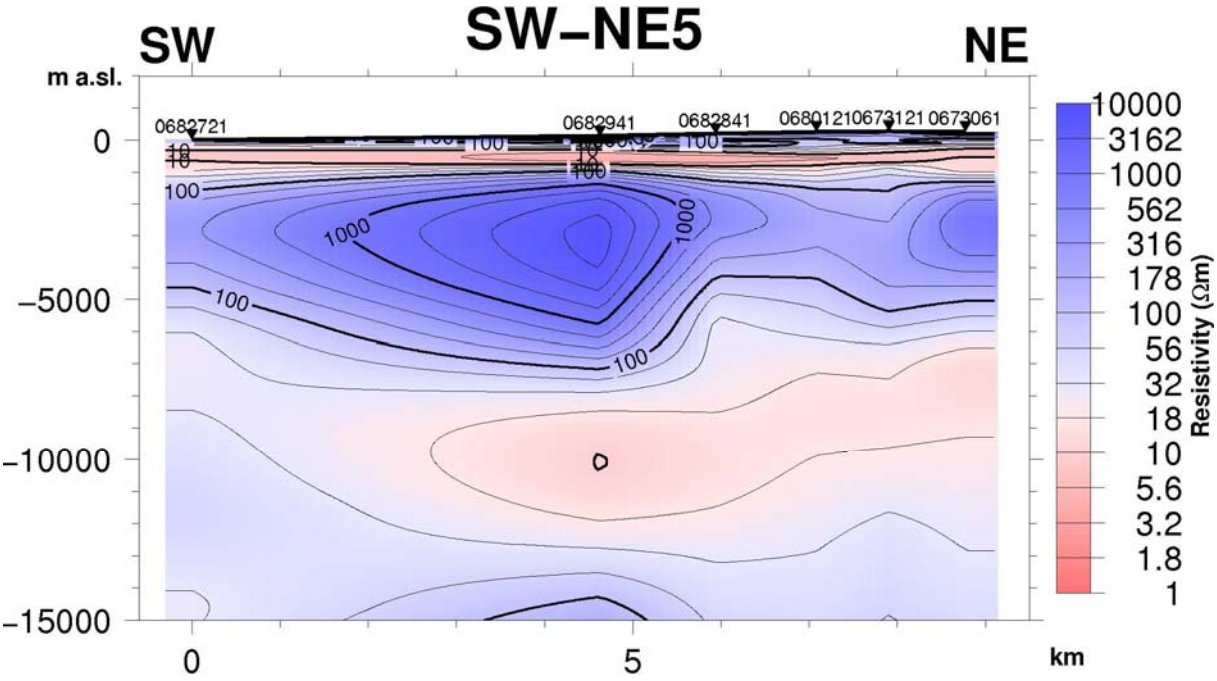

FIGURE 34: MT resistivity cross-section SW-NE5

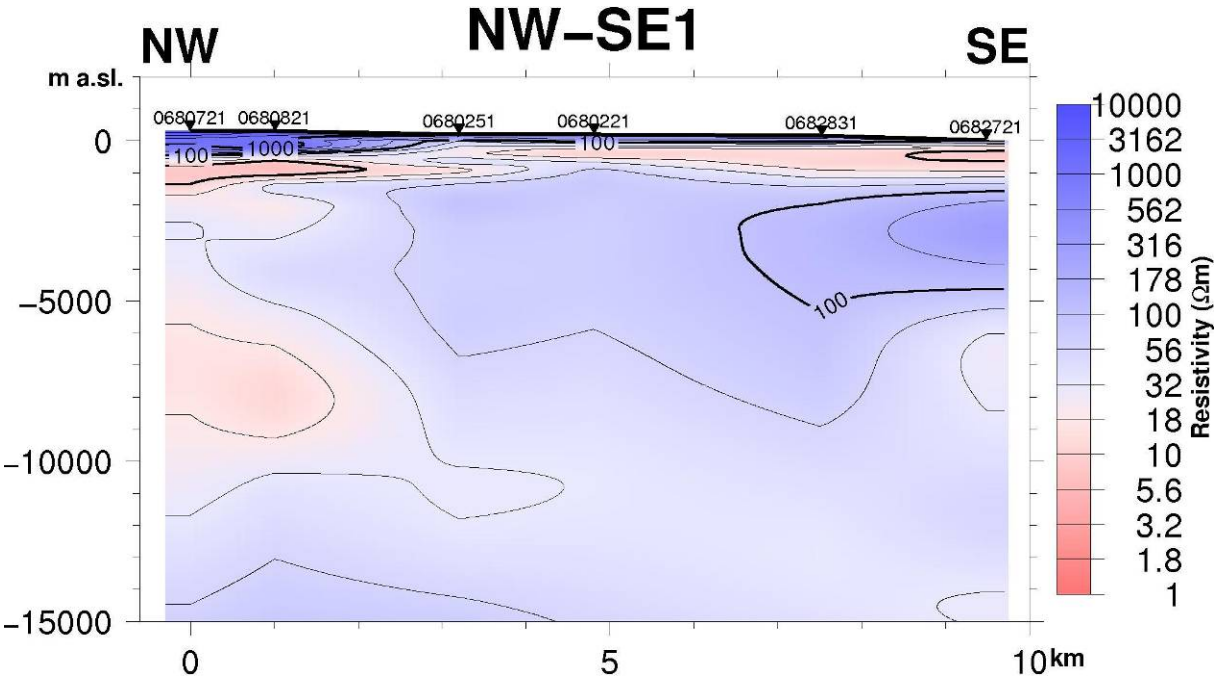

FIGURE 35: MT resistivity cross-section NW-SE1

MT cross-section NW-SE1 (Figure 35) passes across the fissure swarm at the southern end of the prospect area. It shows a low-resistivity layer all along the profile at shallow depth, and another one at depths of 4000-11,000 m b.s.l. on its western side.

The MT cross-section NW-SE2 (Figure 36) passes through the central part of the study area across the fissure swarm. This cross-section cuts the lower low-resistivity layer from about 2500 down to 11,000 m b.s.l., and cuts the highly resistive formation (> 10,000 Ωm), seen in Figure 34, on its eastern side.

MT cross-section NW-SE3 (Figure 37) passes through the northern part of the study area. It shows the lower low-resistivity layer along all the length of the profile but deepening, and with increasing resistivity to the east.

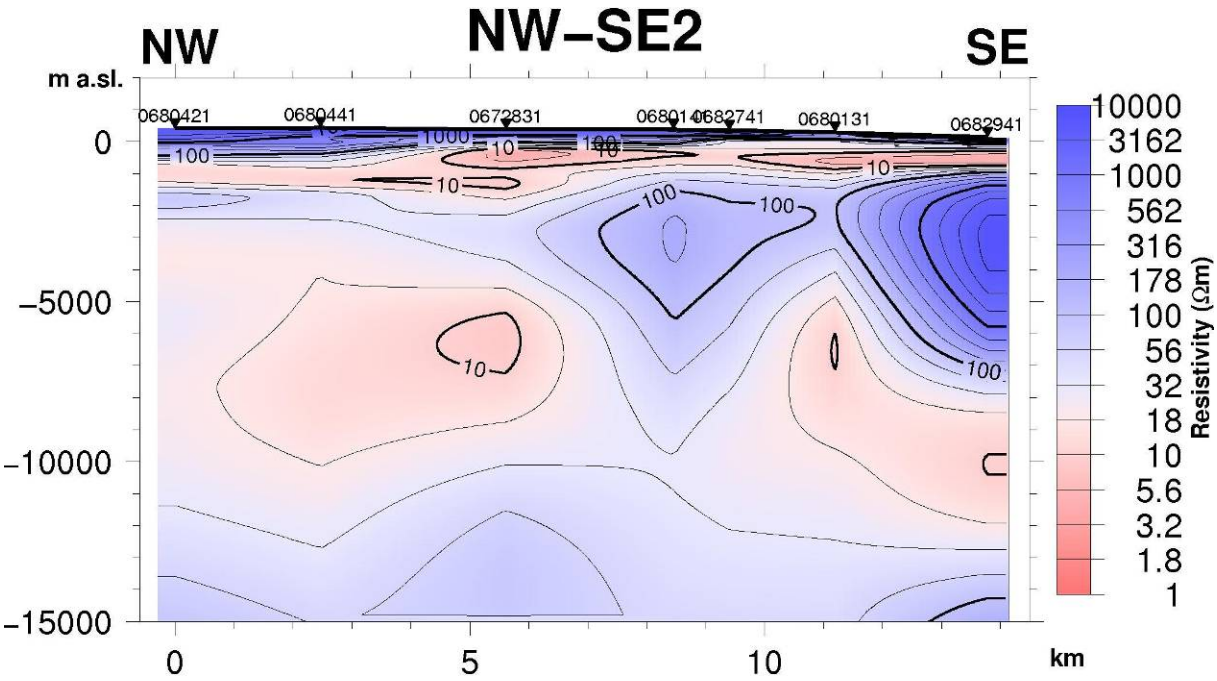

FIGURE 36: MT resistivity cross-section NW-SE2

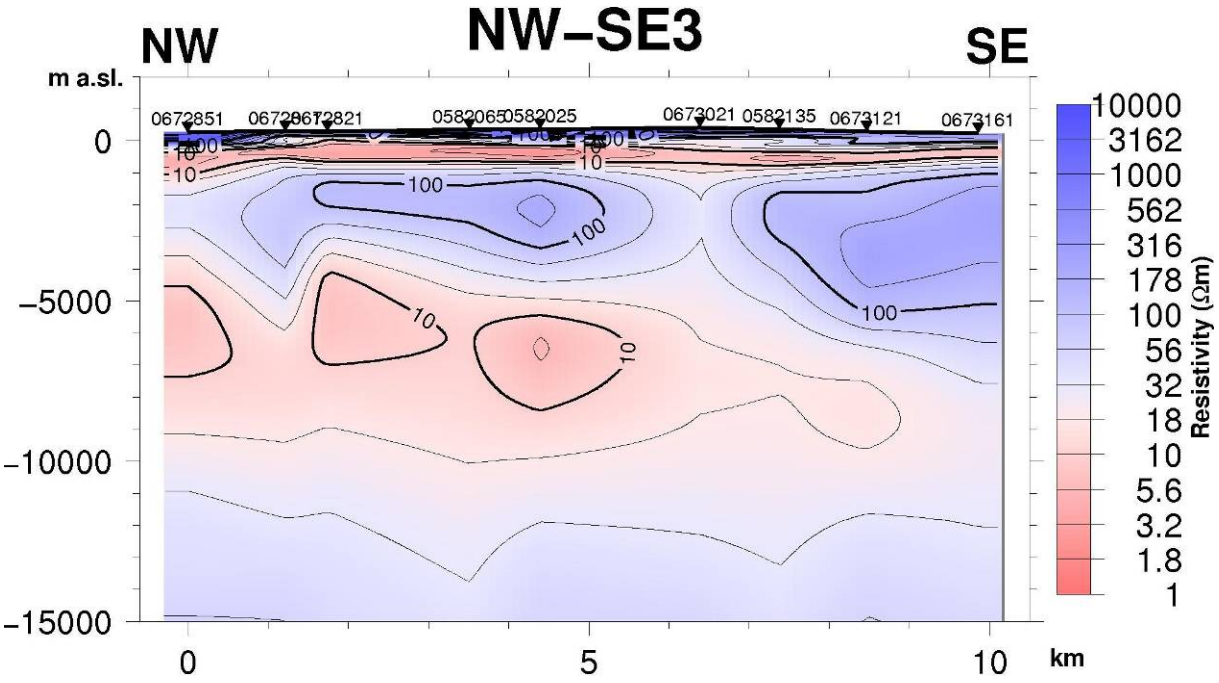

FIGURE 37: MT resistivity cross-section NW-SE3

Finally, as mentioned above, Figure 38 shows a detailed version of the uppermost 1000-1500 m of MT-cross-section SW-NE1. The comparison with the TEM cross-section in Figure 19 shows a very similar resistivity distribution, strengthening the confidence in the results of the MT.

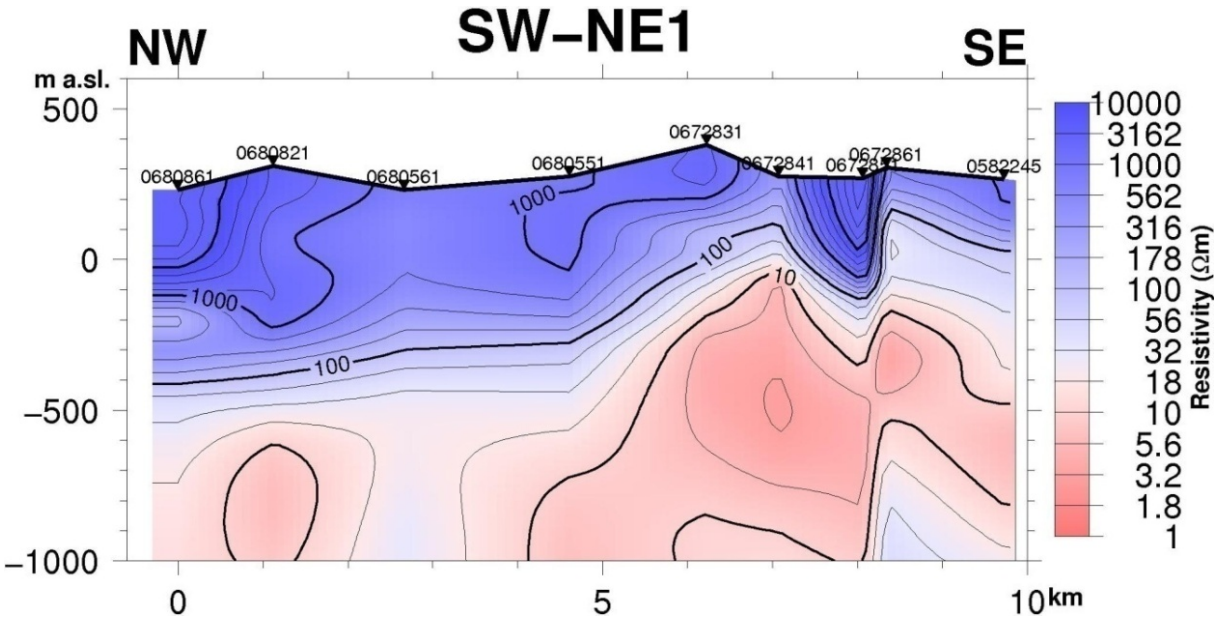

FIGURE 38: The uppermost 1200 m of the MT resistivity cross-section SW-NE1, presented in an exaggerated scale for comparison with the same TEM cross-section

8. CONCLUSIONS

This integrated TEM-MT resistivity survey gives a detailed picture of the resistivity in the southwest part of the Hengill geothermal area. A total of 106 existing TEM soundings and data from 47 MT stations (EDI files) were interpreted. The data interpretation of the TEM/MT data was done using the 1D inversion program TEMTD. The MT data were jointly inverted with TEM data from the same location, to determine the best static shift parameter for the MT data. Static shift of these data sets ranges from 0.5 to 1.3, the majority being around 0.8. The interpreted data are presented in the form of resistivity cross-sections and iso-resistivity maps as well as data curves and layered models.

The results obtained from the TEM and MT surveys in the study area reveal, for TEM, the sequence of resistivity distribution of the rock formation in the uppermost kilometre and, for MT, down to about 15 km. Except along the active fissure swarm, the resistivity in the uppermost few hundred metres, down to approximately 100 m b.s.l. , is quite high ranging between 100 and 10,000 Ωm, and in particular it is high in the western part of the area. This high resistivity can be correlated with fresh unaltered volcanic rocks. Below, to depths of 900 m b.s.l. the resistivity is generally low (1-10 Ωm). This low-resistivity zone can be correlated with the mineral alteration of the smectite-zeolite zone, and it has been referred to as the low-resistivity cap. In addition, a high-resistivity core is also widely observed below the low-resistivity cap, particularly in the TEM resistivity isomaps at 700 and 900 m b.s.l. (Figures 17 and 18). In most of the TEM cross-sections, the top of the high-resistivity core is observed to reach up to 200-300 m b.s.l. At deeper levels, the general resistivity increases, as observed in the MT iso-resistivity maps and cross-sections at about 2000 m b.s.l. This can be associated with the generally higher temperatures at this level and alteration in the chlorite and chlorite-epidote zones. At still deeper levels, MT iso-resistivity maps at 5000-10,000 m b.s.l. and cross-sections show general low resistivity, seen between 3000 and 11,000 m b.s.l., which might be associated with the main heat source for the geothermal system, which above gives rise to the alteration distribution seen associated with a high-resistivity core and a low-resistivity cap. This deep low-resistivity anomaly may reflect partially molten basaltic magma or magmatic brine.

Generally, from the TEM and MT results obtained, it can be concluded that the Hellisheidi geothermal field of Hengill volcanic system has good geothermal potential. If there is equilibrium between the thermal alteration of the rock and the present temperature in the reservoir, the temperatures within the high-resistivity core are expected to exceed 250°C.

ACKNOWLEDGEMENTS

Above all, I would like to thank the almighty God for all his help. I sincerely thank the United Nations University and the Government of Iceland for sponsoring me to participate in the Geothermal Training Programme. My sincere gratitude to Dr. Ingvar B Fridleifsson, Director of UNU-GTP, and Mr. Lúdvík S. Georgsson, Deputy Director, Ms. Thórhildur Ísberg and Mrs. Dorthe H. Holm for their care and help through all the training period. Special thanks to my advisor, Mr. Knútur Árnason, for his invaluable help through excellent lectures and all his guidance and advice from the beginning to the end. I would also like to thank Dr. Hjálmar Eysteinsson for his great assistance and Mrs. Ragna Karlsdóttir for assisting me in correcting and reviewing the manuscript.

I am also very thankful to the Orkustofnun and ÍSOR staff members for their good lectures and assistance in all respects. The UNU-GTP Fellows of 2007 are also greatly acknowledged for sharing their experiences with me. And lastly but not least, I would like to express my gratitude to the Department of Mines, Eritrea for allowing me to participate in this training program.

REFERENCES

Archie, G.E., 1942: The electrical resistivity log as an aid in determining some reservoir C-characteristics. *Tran. AIME, 146,* 54-67.

Árnason, K., 1989: *Central loop transient electromagnetic sounding over a horizontally layered earth*. Orkustofnun, Reykjavík, report OS-89032/JHD-06, 129 pp.

Árnason, K., 2006a: *Further exploration of the south part of the Hengill fissure swarm with resistivity soundings.* ÍSOR, Reykjavík, report ÍSOR-06118 (in Icelandic), 19 pp.

Árnason, K., 2006b: *TEMTD (Program for 1D inversion of central-loop TEM and MT data)*. ÍSOR, Reykjavík, short manual 16, pp.

Árnason, K., Björnsson, G., Flóvenz, Ó.G., and Haraldsson, E.H., 1988: *Geothermal resistivity survey in the Asal Rift in Djibouti.* Orkustofnun, report OS-88301/JHD-05 prepared for UND-OPS and ISERT, I, 48 pp.

Árnason, K., and, Flóvenz, Ó.G., 1992: Evaluation of physical methods in geothermal exploration of rifted volcanic crust. *Geothermal Resources Council, Transactions*, *16*, 207-213.

Árnason, K., Haraldsson, G.I., Johnsen, G.V., Thorbergsson, G., Hersir, G.P., Saemundsson, K., Georgsson, L.S., Rögnvaldsson, S.Th., and Snorrason, S.P., 1987: *Nesjavellir-Ölkelduháls, surface exploration 1986.* Orkustofnun, Reykjavík, report OS-87018/JHD-02 (in Icelandic), 112 pp + maps.

Árnason, K., Karlsdóttir, R., Eysteinsson, H., Flóvenz, Ó.G., and Gudlaugsson, S.Th., 2000: The resistivity structure of high-temperature geothermal systems in Iceland. *Proceedings of the World Geothermal Congress 2000*, *Kyushu-Tohoku, Japan,* 923-928.

Cagniard, L., 1953: Basic theory of the magneto-telluric method of geophysical prospecting. *Geophysics, 18,* 605-635.

Dakhnov, V.N., 1962: *Geophysical well logging*. Q. Colorado Sch. Mines*,* 57-2, 445 pp.

Eysteinsson, H., 2007: *The resistivity drawing programs TEMRESD and TEMCROSS.* ÍSOR, Reykjavík, unpublished.

Eysteinsson, H., Árnason, K., and Flóvenz, Ó.G., 1993: Resistivity methods in geothermal prospecting in Iceland. *Surveys in Geophysics, 15,* 263-275.

Flóvenz, Ó.G., Georgsson, L.S., and Árnason, K., 1985: Resistivity structure of the upper crust in Iceland. *J. Geophys. Res., 90-B12,* 10,136-10, 150.

Franzson, H., Kristjánsson, B.R., Gunnarsson, G., Björnsson, G., Hjartarson, A., Steingrímsson, B., Gunnlaugsson, E., and Gíslason G., 2005: The Hengill Hellisheidi geothermal field. Development of a conceptual geothermal model. *Proceedings of the World Geothermal Congress 2005, Antalya, Turkey,* CD, 7 pp.

Fridleifsson, G.Ó, Ármannsson, H., Árnason, K., BjÁrnason, I.Th., and Gíslason, G., 2003: Part I: Geosciences and site selection. In: Fridleifsson, G.Ó. (ed.), *Iceland Deep Drilling Project, feasibility report.* Orkustofnun, Reykjavik, report OS-2003-007, 104 pp.

Hermance, J.F., 1973: Processing of magnetotelluric data. *Physics of the Earth and Planetary Interiors, 7,* 349-364.

Hersir, G.P., and Björnsson, A., 1991: *Geophysical exploration for geothermal resources. Principles and applications*. UNU-GTP, Iceland, report 15, 94 pp.

Jones, A.G., 1988: Static shift of magnetotelluric data and its removal in a sedimentary basin environment. *Geophysics, 53-7*, 967-978.

Keller, G.V., and Frischknecht, F.C., 1966: *Electrical methods in geophysical prospecting.* Pergamon Press Ltd., Oxford, 527 pp.

Manzella, A., 2006: *Geophysical methods in geothermal exploration*. Italian National Research Council, International Institute for Geothermal Research, Pisa. Internet webpage: *cabierta.uchile.cl/revista/12/articulos/pdf/A_Manzella.pdf,* 40 pp.

McNeill, 1980: Applications of transient electromagnetic techniques. Geonics Ltd., Ontario, Technical note TN-7, 17 pp.

Oskooi, B., 2006: 1D interpretation of the magnetotelluric data from Travale geothermal field in Italy. *J. of the Earth and Space physics, 32-2,* 16 pp.

Pellerin, L., and Hohmann, G.W., 1990: Transient Electromagnetic Inversion: A remedy for magnetotelluric static shifts. *Geophysics*, *55-9*, 1242-1250.

Phoenix Geophysics, 2005: *Data processing. User's guide.* Phoenix Geophysics, Ltd.,Toronto.

Quist, A.S., and Marshall, W.L., 1968: Electrical conductances of aqueous sodium chloride solutions from 0 to 800°C and at pressures to 4000 bars. *J. Phys. Chem., 72,* 684-703.

Rink, M. and Shopper, J.R. 1976: Pore structure and physical properties of porous sedimentary rocks. *Pure & Appl. Geophys, 114,* 273-284.

Saemundsson, K., 1967: Vulkanismus und Tektonik des Hengill-Gebietes in Sudwest-Island (in German). *Acta Nat. Isl., II-7*, 195 pp.

Saemundsson, K., 1995: *Geological map of the Hengill area 1:50,000*. Orkustofnun, Reykjavík.

Ward, S.H, and Wannamaker, P.E., 1983: *The MT/AMT electromagnetic method in geothermal exploration.* UNU-GTP, Iceland, report 5, 107 pp.

APPENDIX I: Examples of plots of 1D modelling of TEM sounding data

The measured TEM data curve is shown with red (dark) dots; the calculated TEM data curve is a black line connecting the red (dark) dots, and the 1D layered modelling is in green (gray).

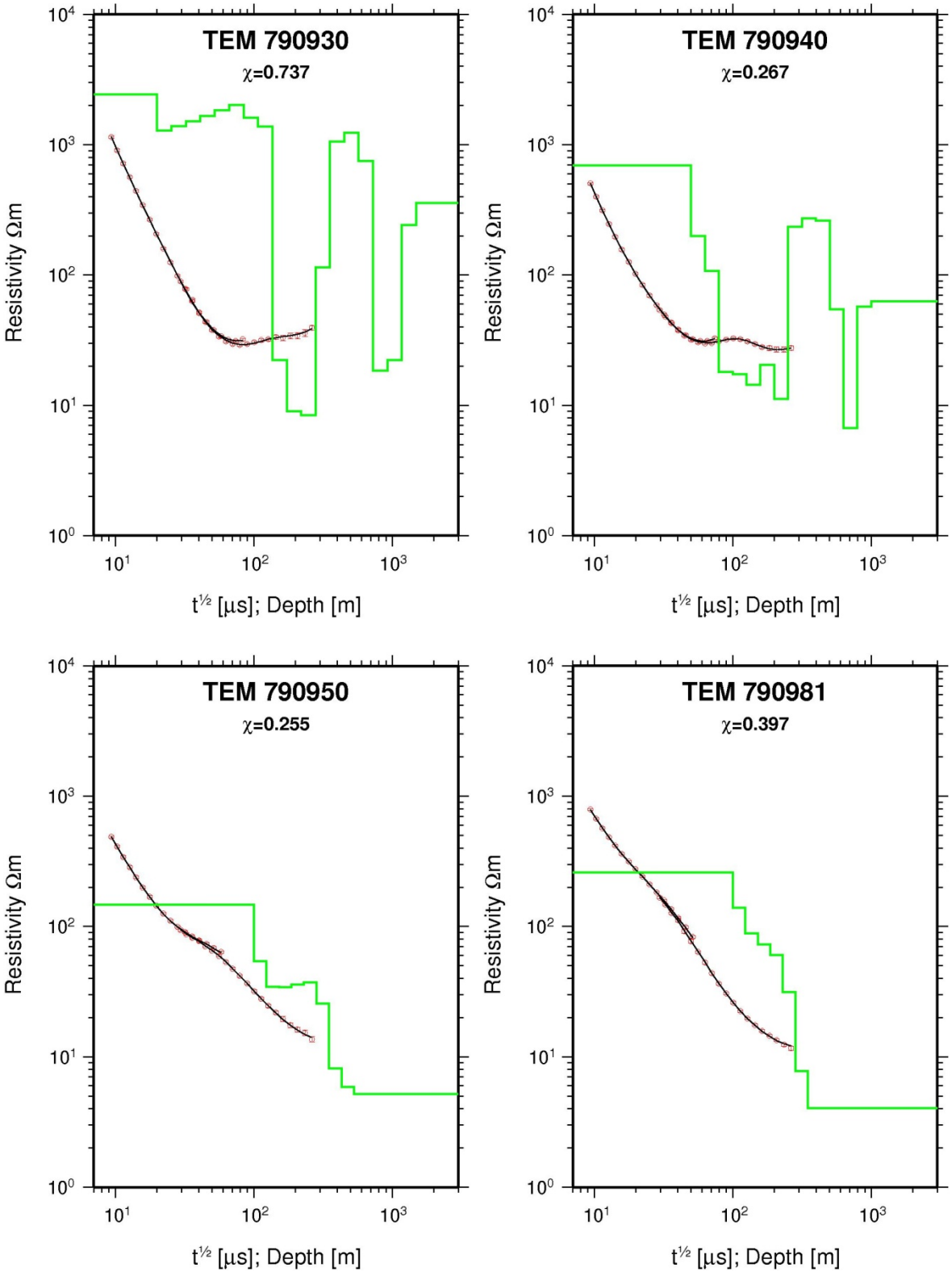

APPENDIX II: Examples of plots of 1D modelling of MT and TEM jointly inverted sounding data

The red (dark) line represents the TEM curve and blue (gray) represents the MT curve. The green (gray) line to the right represents 1D layered resistivity modelling.